Heavy-Ion Beam Dynamics in the RIA Accelerators and Development of RT Accelerating Structures for the RIA

- Layout of the RIA accelerators.
- Acceleration of multiple-charge state heavy-ion beams.
- Driver Linac:
  - Injector system: ECR-LEBT-RFQ;
  - Design of 57.5 MHz cw RFQ;
  - Parametric resonance of transverse motion;
  - Beam steering compensation and electric field symmetry in SRF cavities;
  - Beam Dynamics optimization and simulation;
  - Isopath transport of multi-q beams;
  - BD in high-β section: Triple-Spoke vs Elliptical cavities.
- Design of the Post-Accelerator:
  - RT accelerating structures and beam dynamics.
- Summary and outlook.

Rare Isotope Accelerator Facility

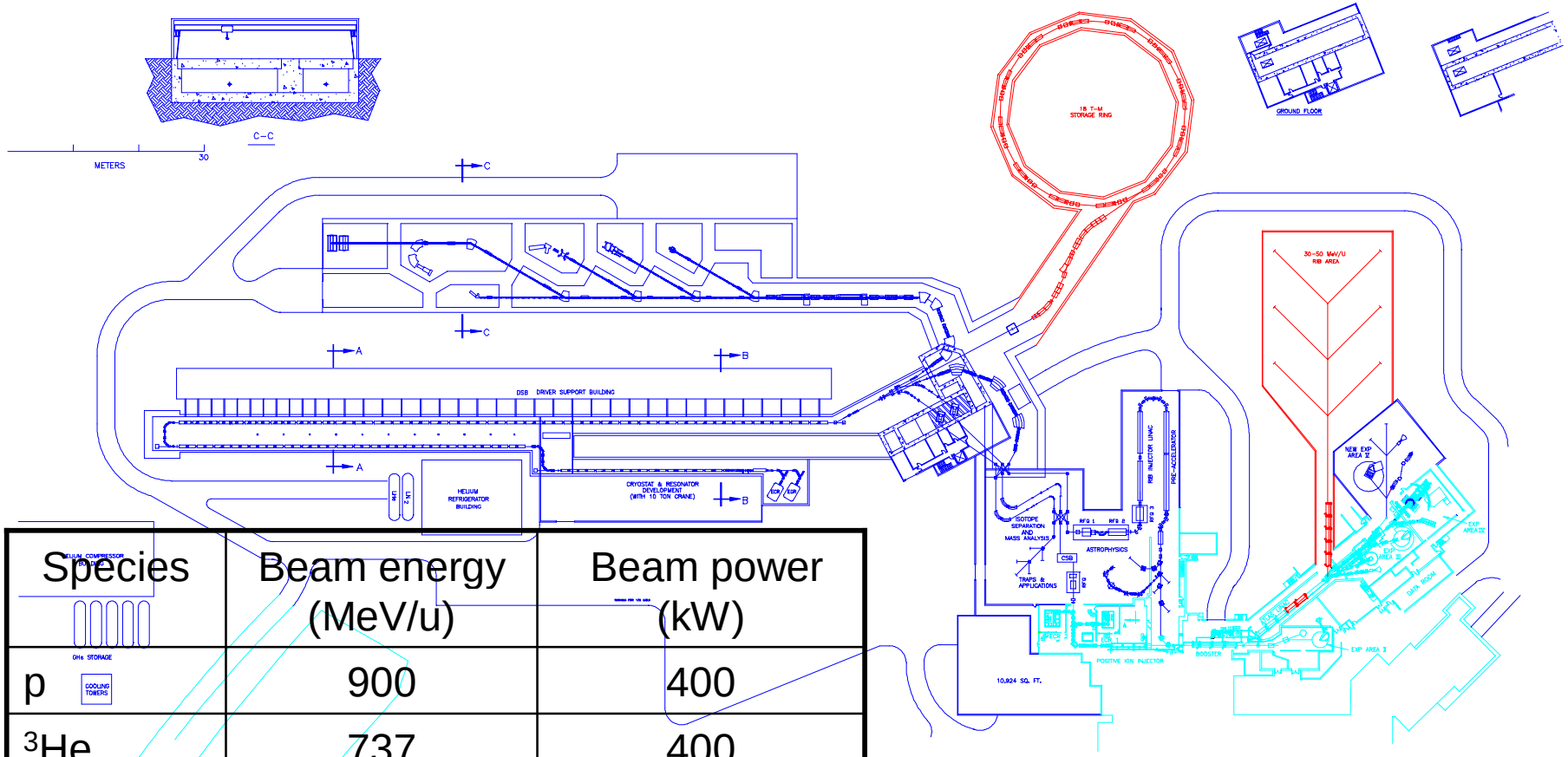

Species	Beam energy (MeV/u)	Beam power (kW)
p	900	400
^{3}He	737	400
^{136}Xe	451	400
^{238}U	400	100 (400)

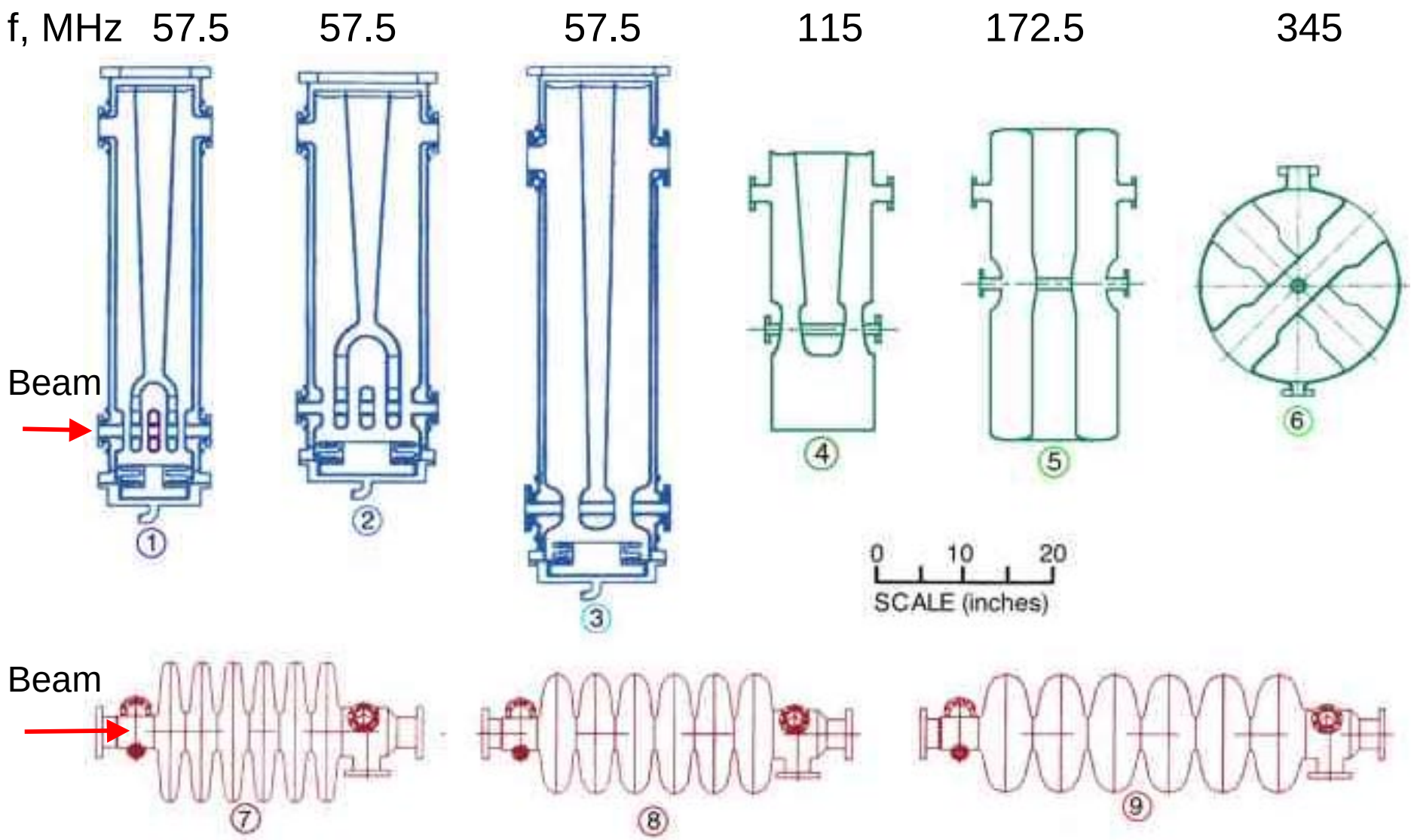
f, MHz 57.5 57.5 57.5 115 172.5 345
Beam
1
2
3
4
5
6
0 10 20
SCALE (inches)
Beam
7
8
9
f, MHz 805 805 805

ANL spoke cavity

JLAB elliptical cavity

Acceleration of synchronous particle

$$\Delta W_{s,u} = \frac{q}{A} eE_0 TL_c \cos\varphi_s$$

Fixed velocity profile
(RFQ, RT DTL)

$$\frac{q}{A}E_0 = const, \quad E_0 = \frac{const}{q/A}$$

Variable velocity profile
(SC Linac)

E_0=const,
Tune phases of individual cavities

Multi-q heavy-ion
accelerator

$$\frac{q_n}{A}E_0 \cos\varphi_{sn} = const, \quad \cos\varphi_{sn,q_n} = \frac{const}{\frac{q_n}{A}E_0}$$

$$\frac{q_n}{A}\cos\varphi_{sn} = \frac{q_0}{A}\cos\varphi_{s,0}$$

Synchronous phase as a function of uranium ion charge state. The designed synchronous phase is –30° for q_0=75.

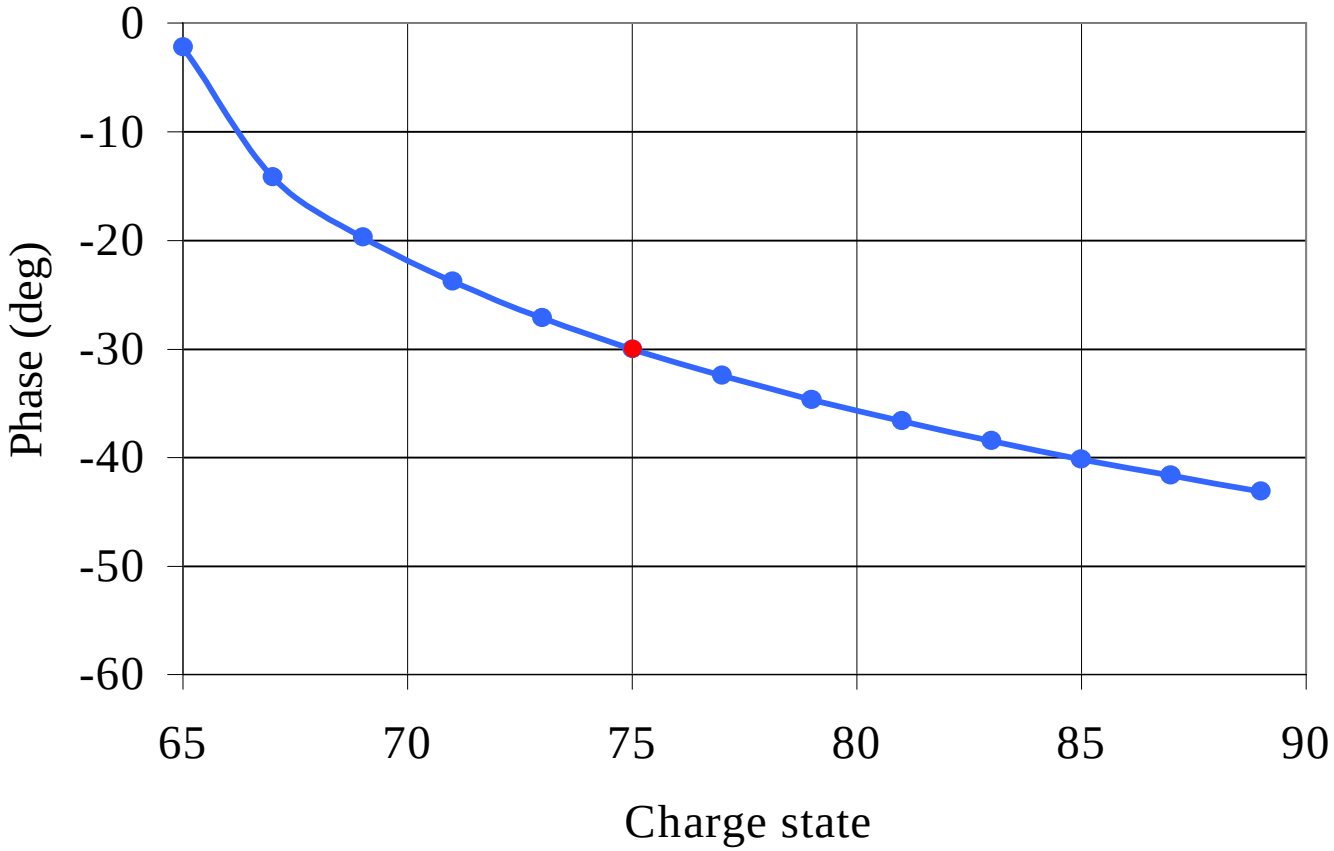

Single accelerating gap

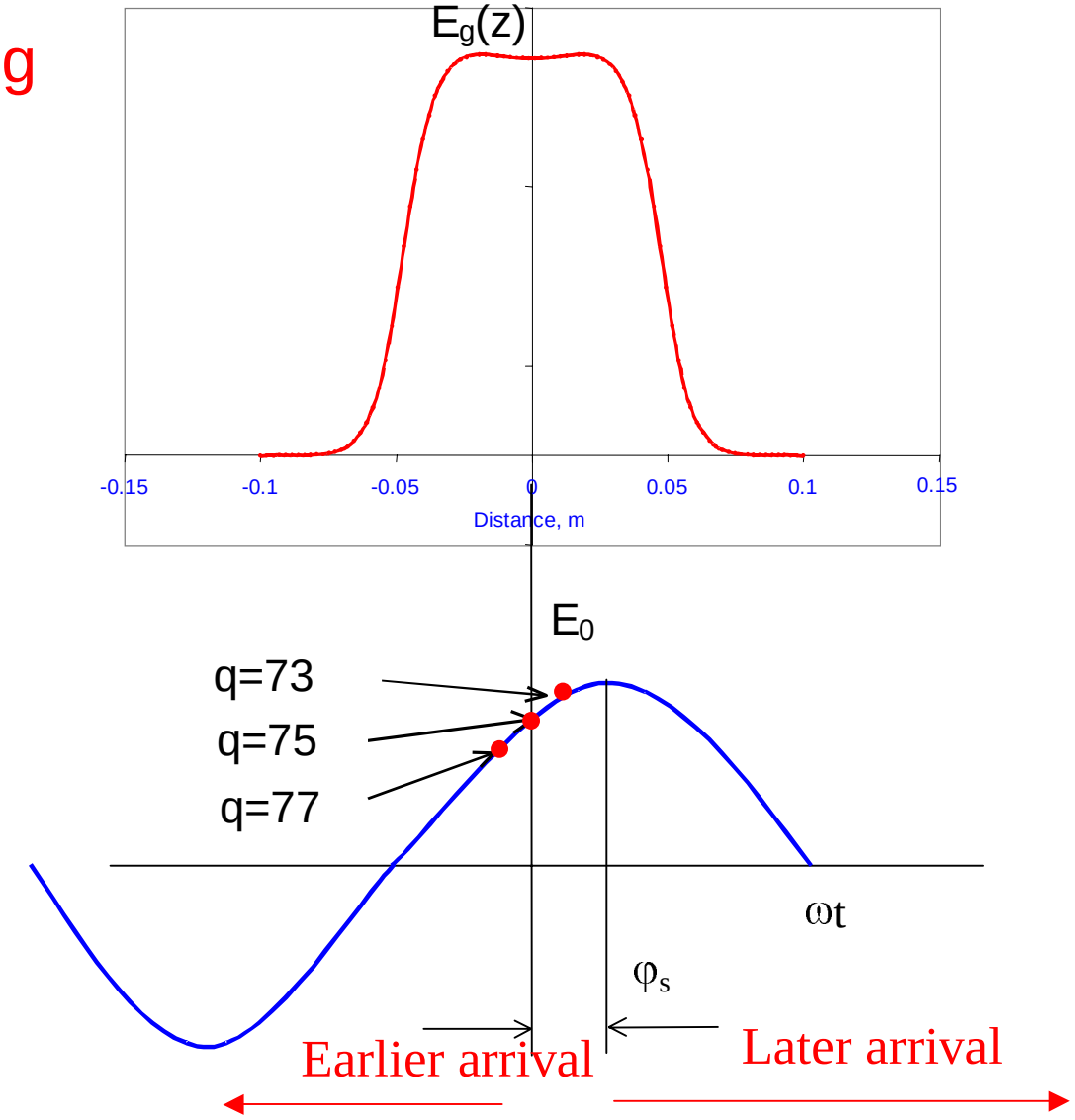

Separatrix and small longitudinal oscillations

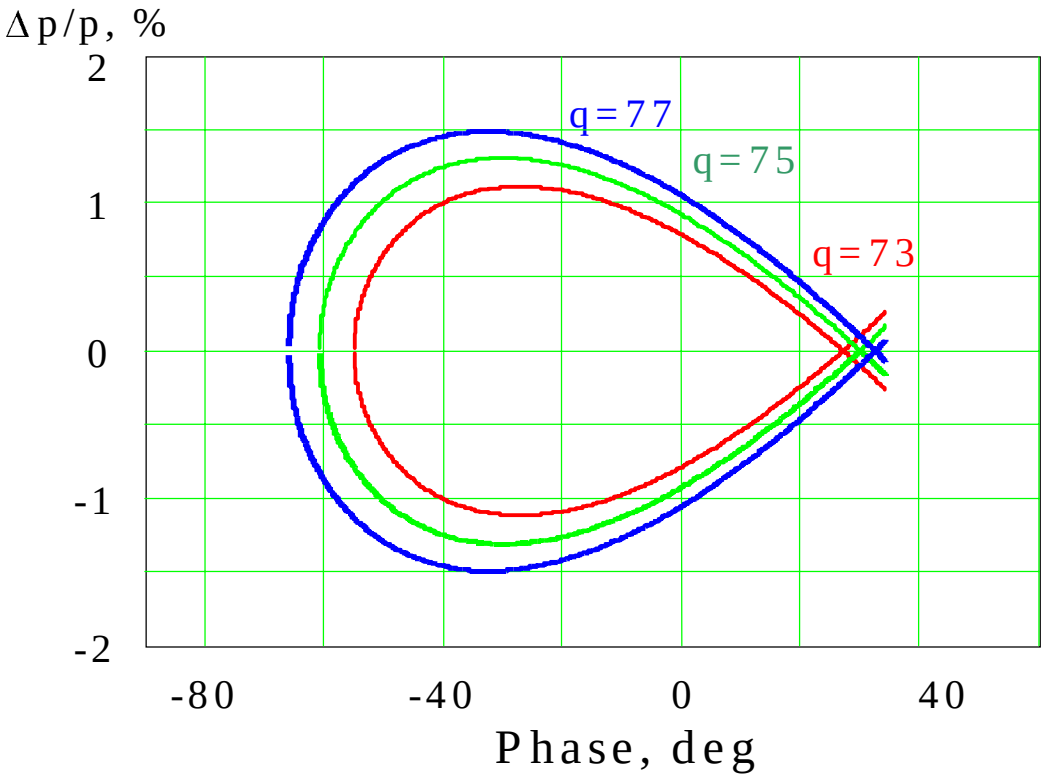

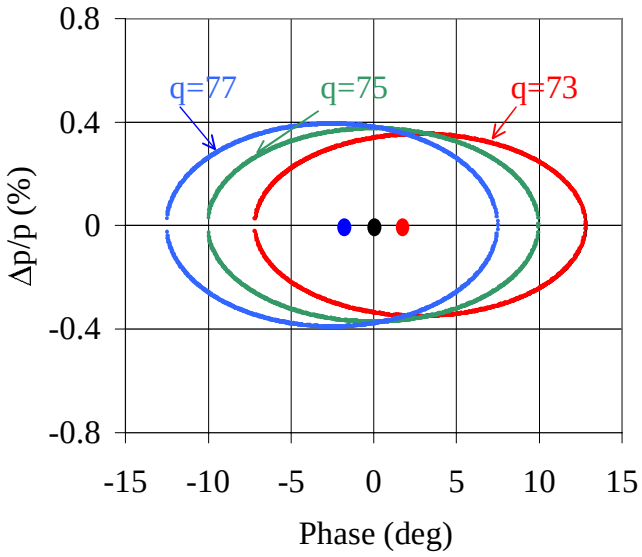

Transverse beam dynamics

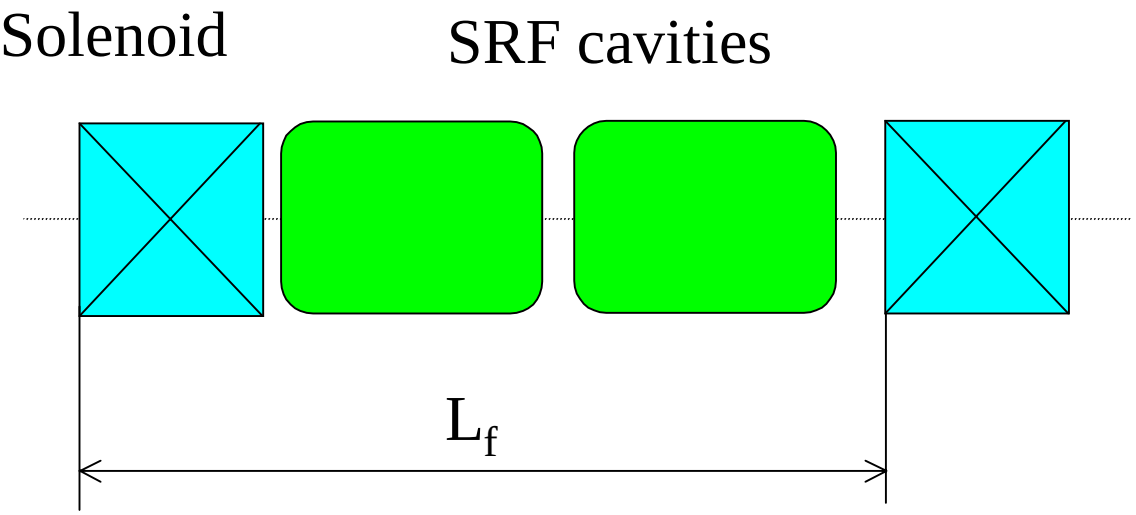

$$M = \begin{bmatrix} \cos\ \mu_x + \alpha_x \sin\ \mu_x & \beta_x \sin\ \mu_x \\ -\gamma_x \sin\ \mu_x & \cos\ \mu_x - \alpha_x \sin\ \mu_x \end{bmatrix}$$

$$\gamma_x x^2 + 2\alpha_x x x' + \beta_x x'^2 = \varepsilon_x$$

Phase advance over the period μ_x and total phase advance Φ_x (modulo 360°) in the medium-beta section (12 MeV/u – 85 MeV/u)

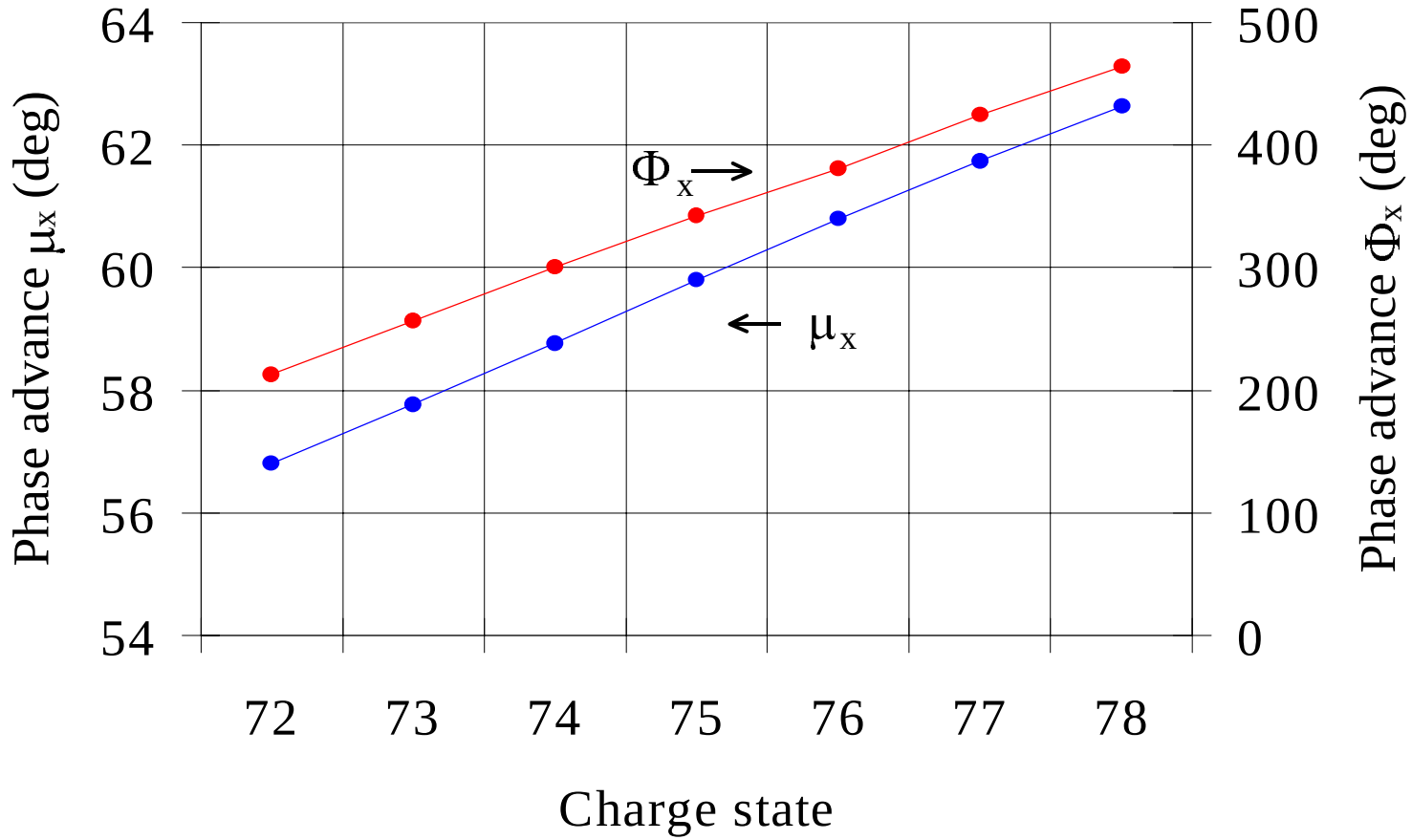

Transverse emittance growth in the focussing channel with alignment errors (±300 μm)

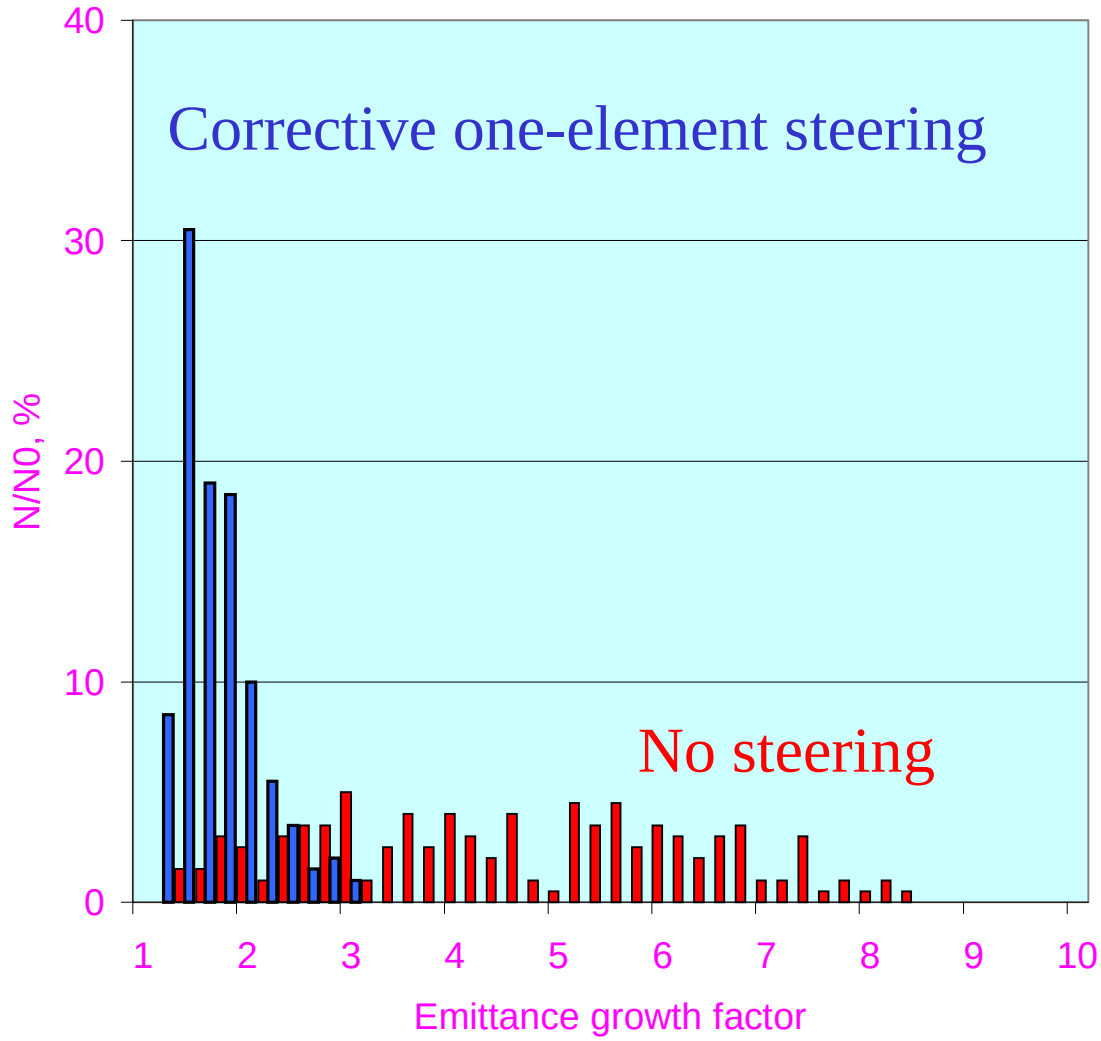

Multi-q beam experiment on ATLAS (ANL)

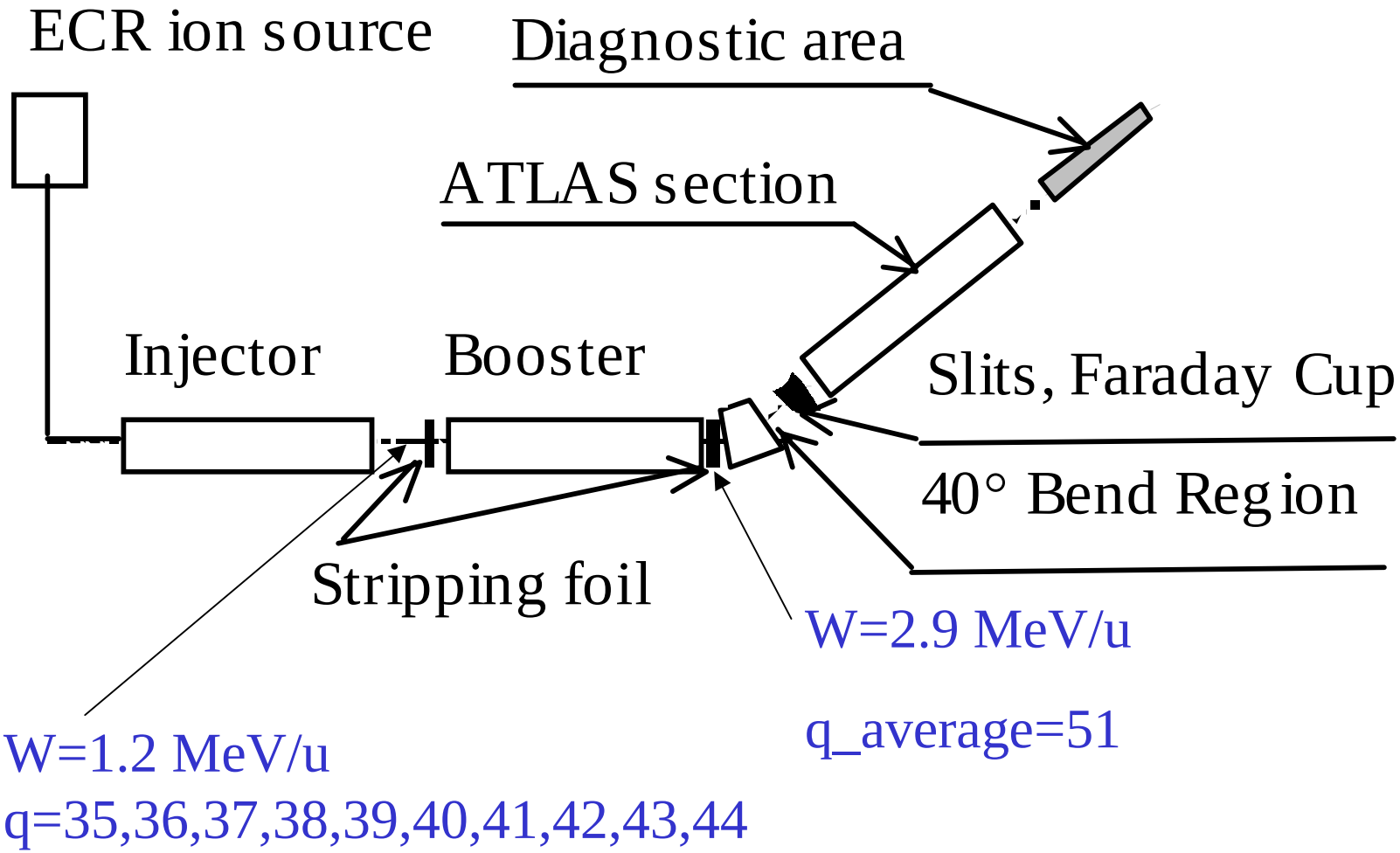

Beam Dynamics Simulations

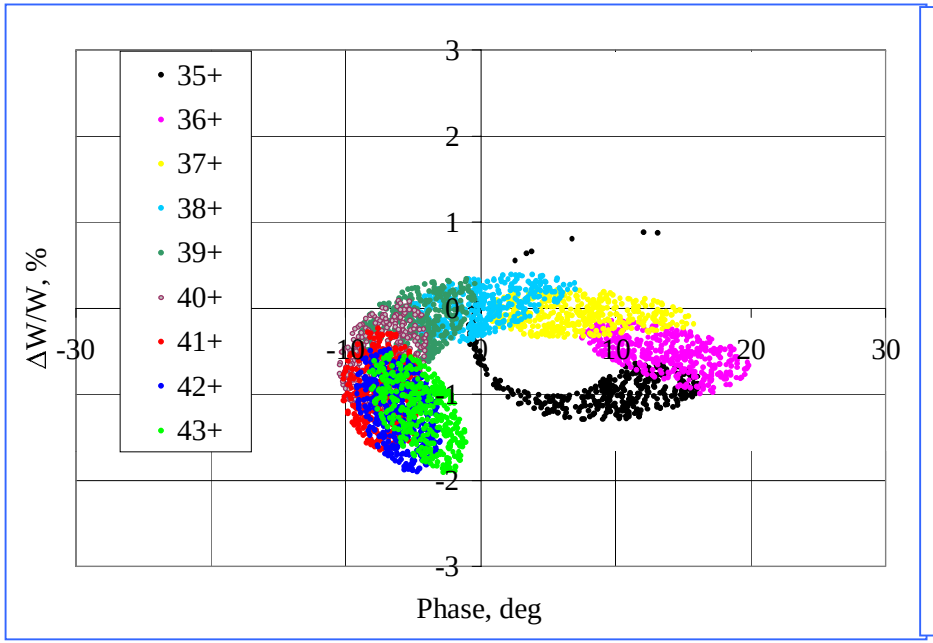

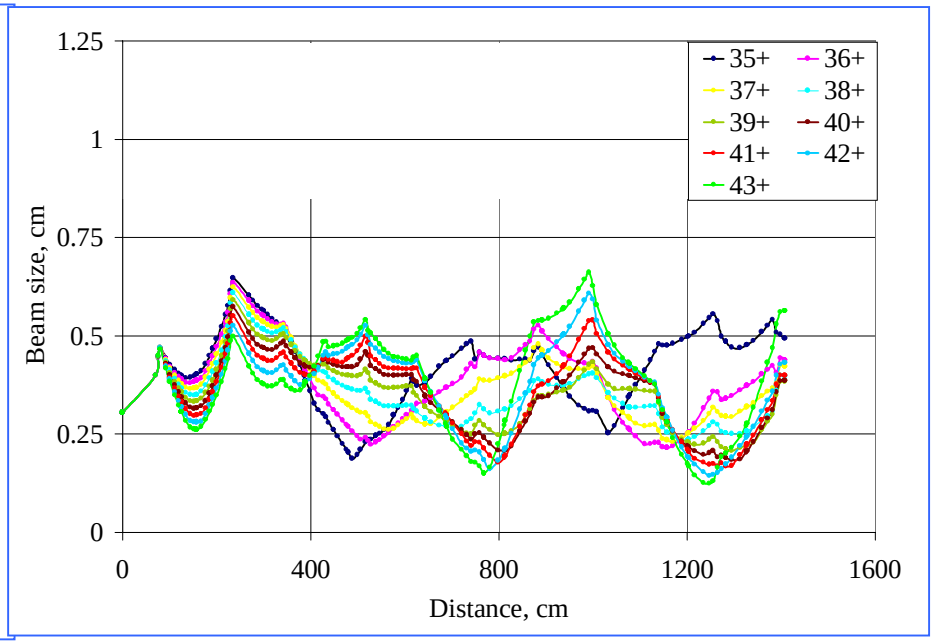

Multi-q beam energy at the exit of the Booster

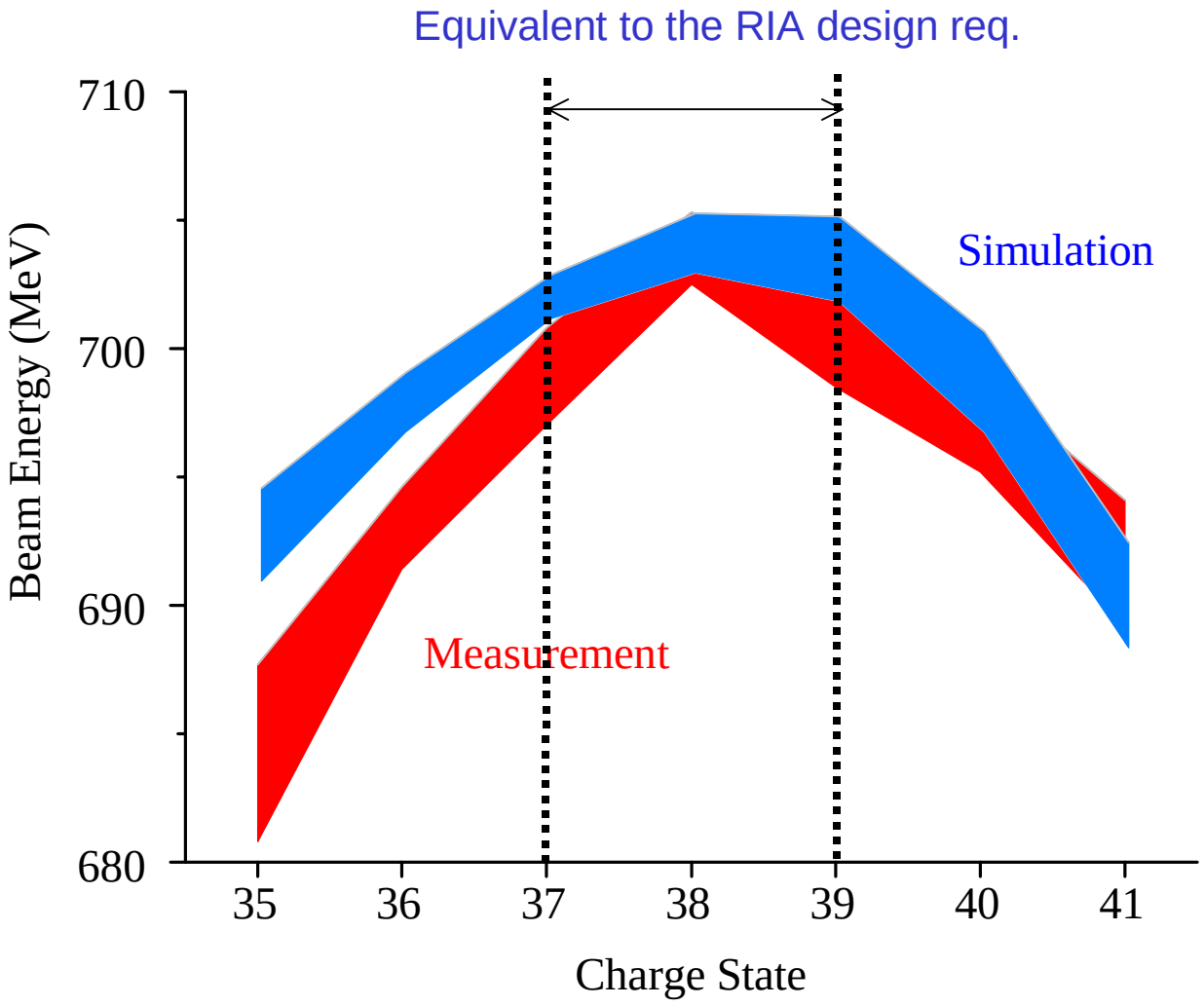

94% **Transmission of Multi-Q Accelerated Beam Through the Booster**

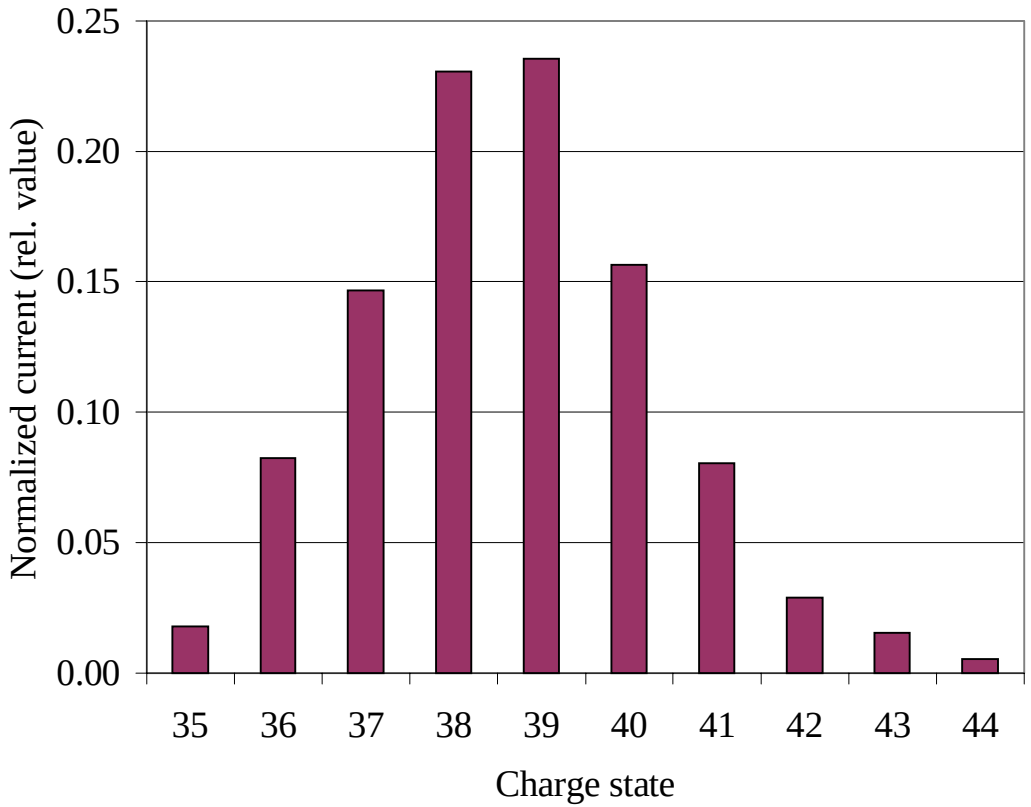

Accelerating and Focusing Lattice of the Driver Linac

Acceleration:

- Superconducting resonators except in the Front End.

Focusing:

- In the DTL: superconducting solenoids.
- In the high-β linac: warm SNS-type quadrupole doublets (baseline design) or SC solenoids.
- Length of focusing period is determined by the stability conditions and required small beam size for high-intensity ion linacs:
  - DTL: $R_{aperture}/R_{rms\_beam} = 11\text{-}12$
  - High-β linac: $R_{aperture}/R_{rms\_beam} = 20\text{-}25$

Layout of the Driver Linac

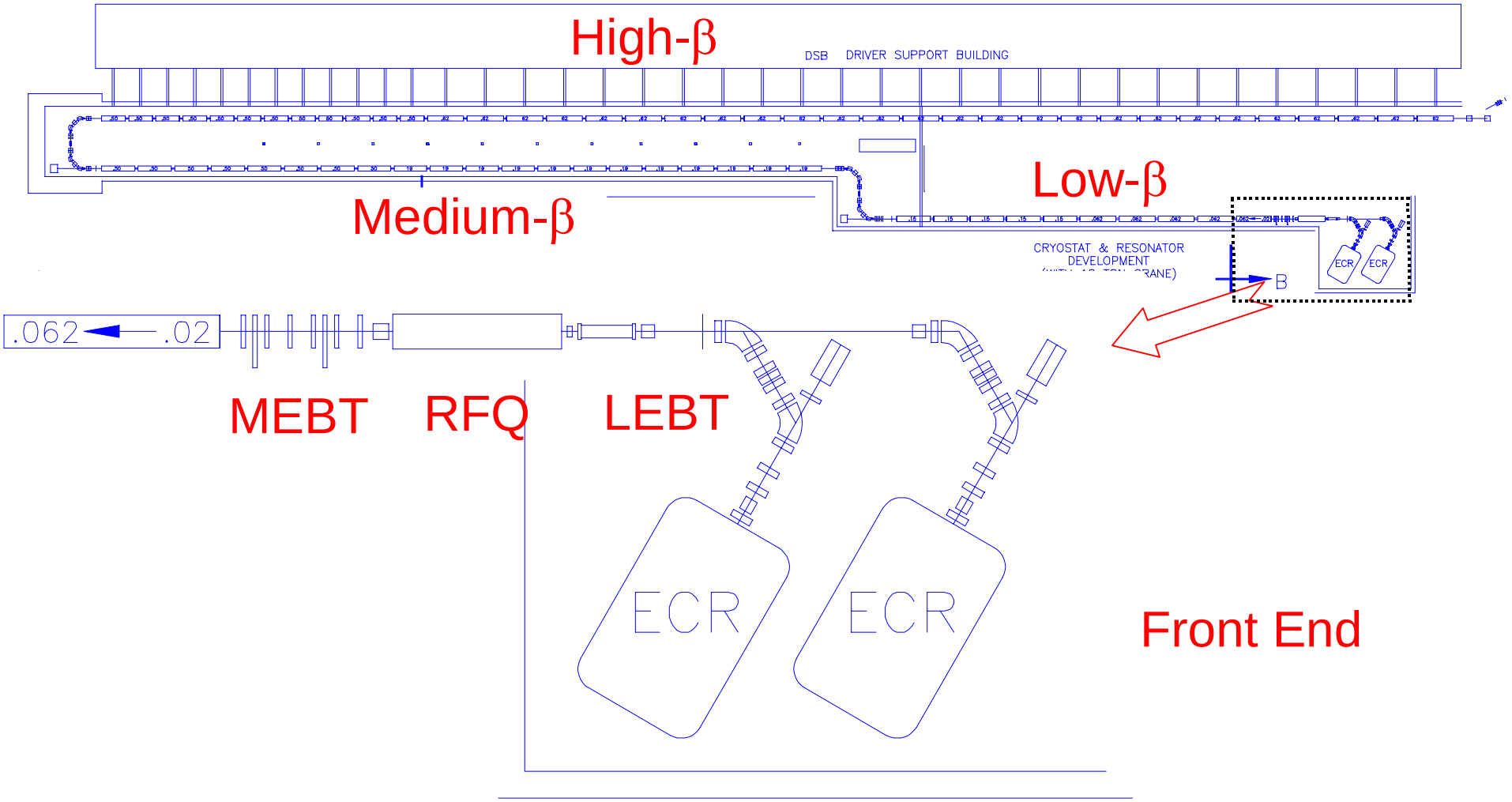

Low-energy achromatic 120° bend

Phase space plots

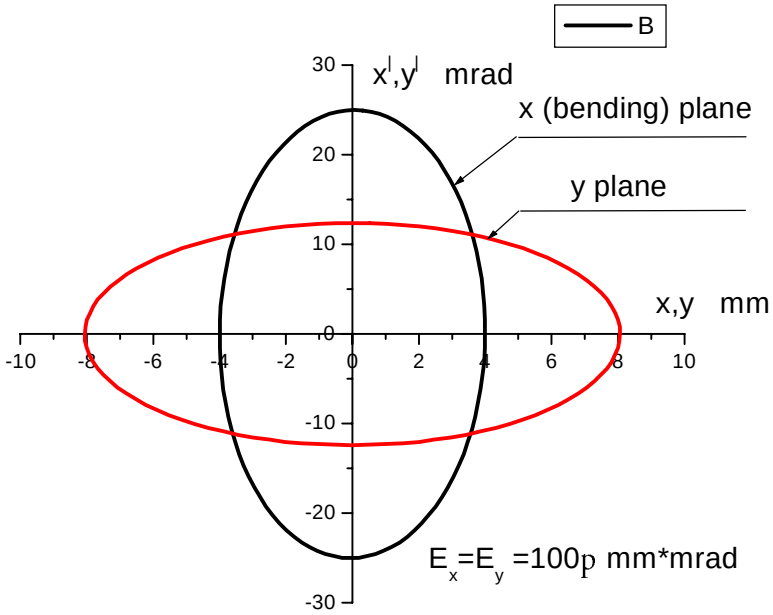

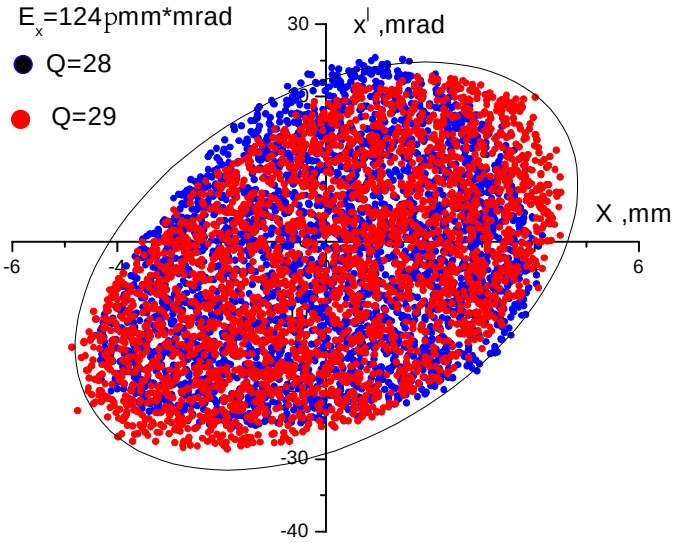

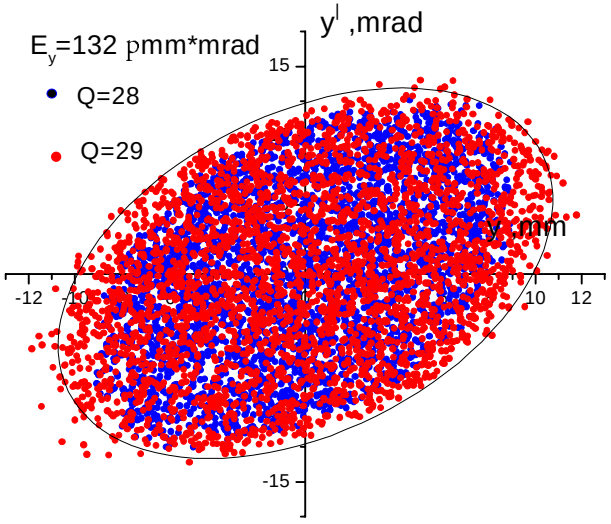

Longitudinal phase space plots of two-charge state uranium beam along the LEBT

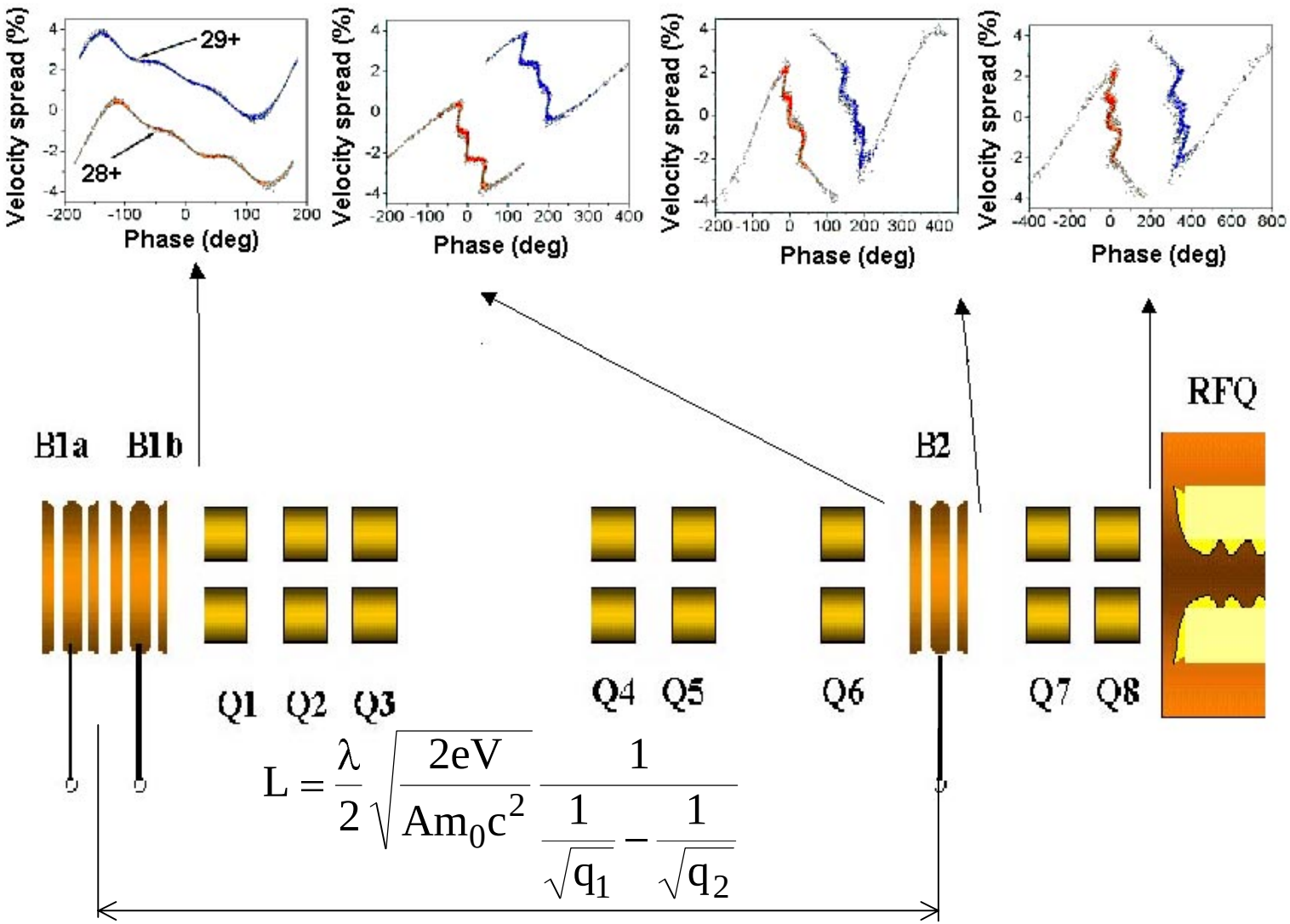

Basic features of the 57.5 MHz RFQ

- CW regime;
- Wide dynamic range of rf power level from $P_0/70$ to P_0 for acceleration of various ion species from protons to uranium;
- Simultaneous acceleration of two charge-state heavy-ion beams;
- Maintaining an extremely small longitudinal emittance formed by the external multi-harmonic buncher;
- Exit of the RFQ: beam waist in both H- and V-planes for easer matching to the following MEBT.

RFQ design options

- Adiabatic bunching;
- Internal ‘klystron’ bunching;
- External multi-harmonic buncher: Extremely low long. emittance (ISAC-1 RFQ, TRIUMF). Simultaneous acceleration of 2 charge states for heavy ions.

Frequency is 57.5 MHz:

a) High-efficiency SRF cavities for the following acceleration;

b) Moderate peak surface fields in the RFQ to provide reliable operation in CW mode;

c) High quality two-charge-state beam parameters;

d) Large transverse acceptance.

e) Possibility to increase inter-vane voltage to accept lower charge states (higher intensities!).

Accelerating by an RFQ

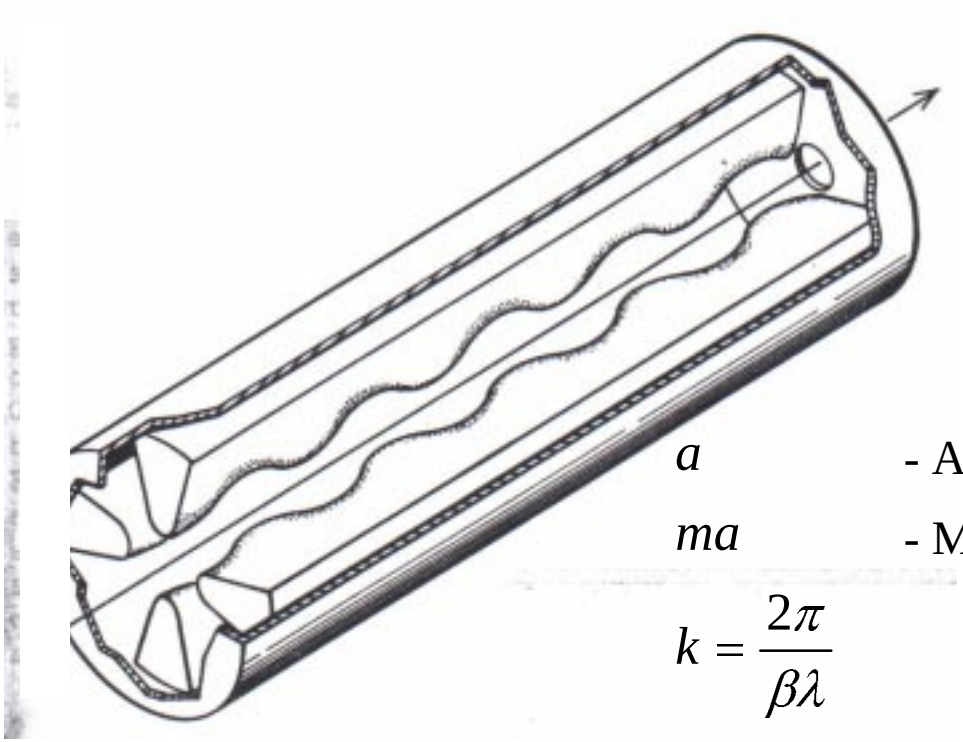

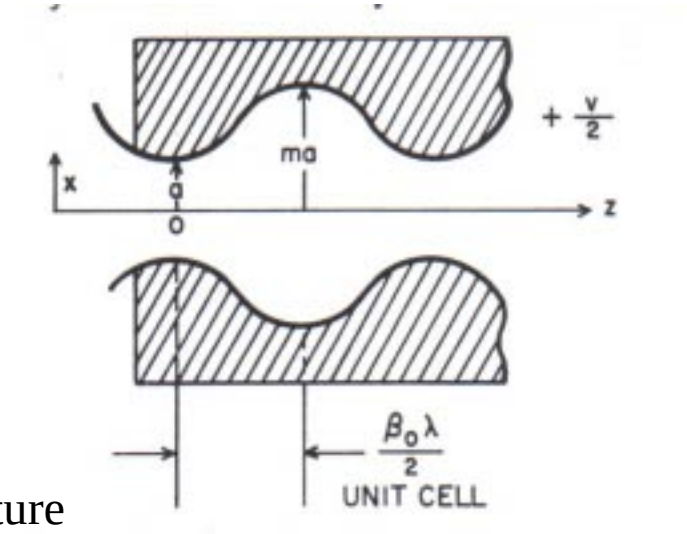

a - Aperture

ma - Maximum distance from axis to electrodes

$$k = \frac{2\pi}{\beta\lambda}$$

$$R_0 = \frac{2a}{m+1}$$

$$L_c = \frac{\beta\lambda}{2}$$

RFQ resonant structure

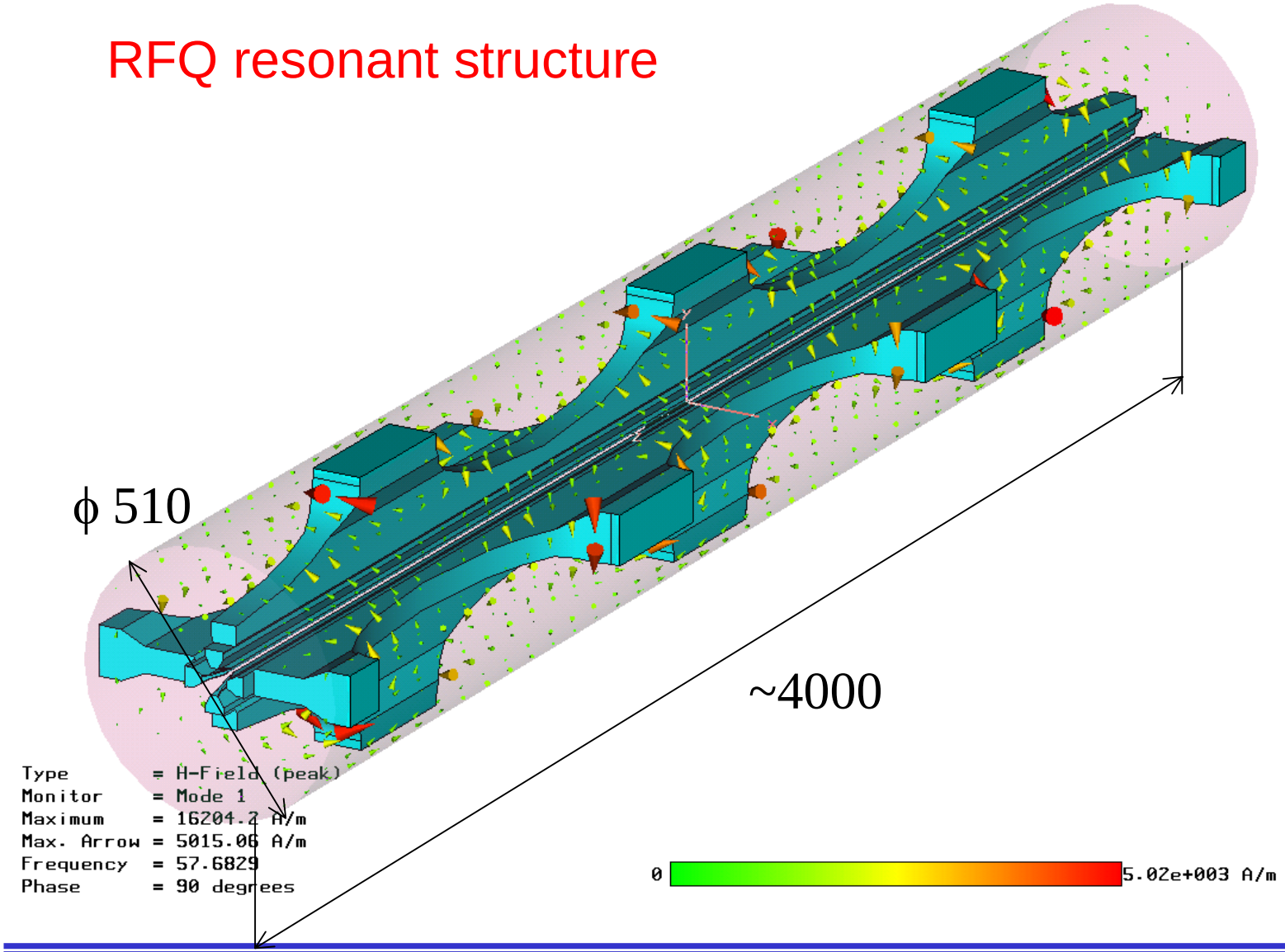

Vane Tip

Longitudinal modulation

$$x = R_0\left(1 + \frac{m-1}{m+1}\sin kz\right)$$

$$y = R_0\left(1 - \frac{m-1}{m+1}\sin kz\right)$$

Transverse cross-section

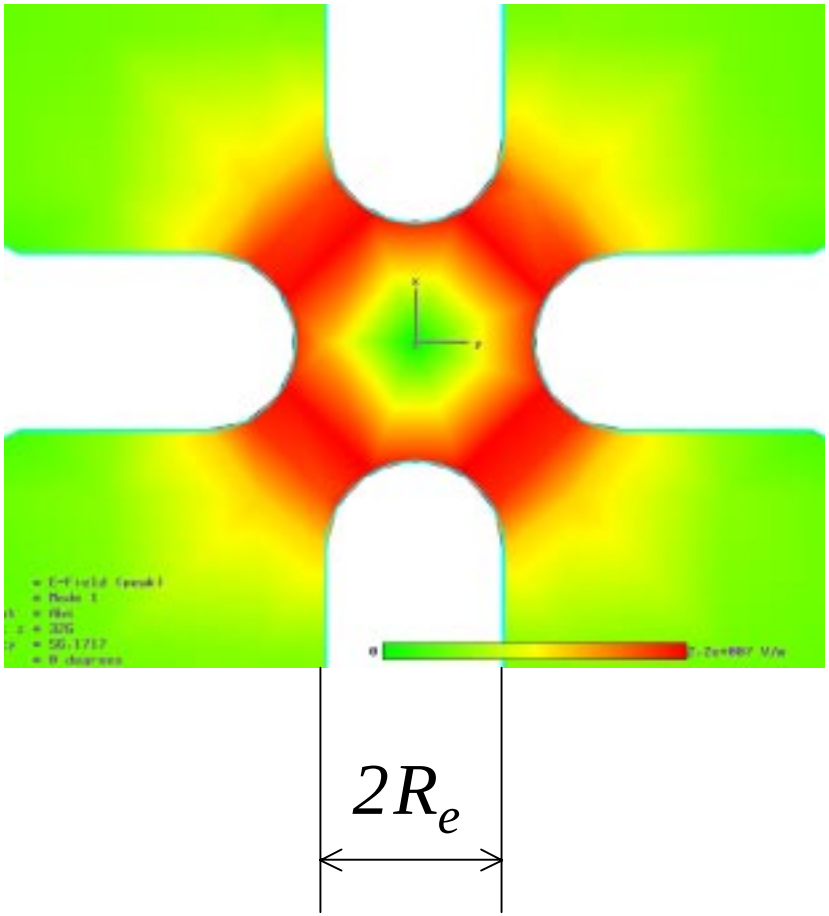

Electric field distribution along the RFQ

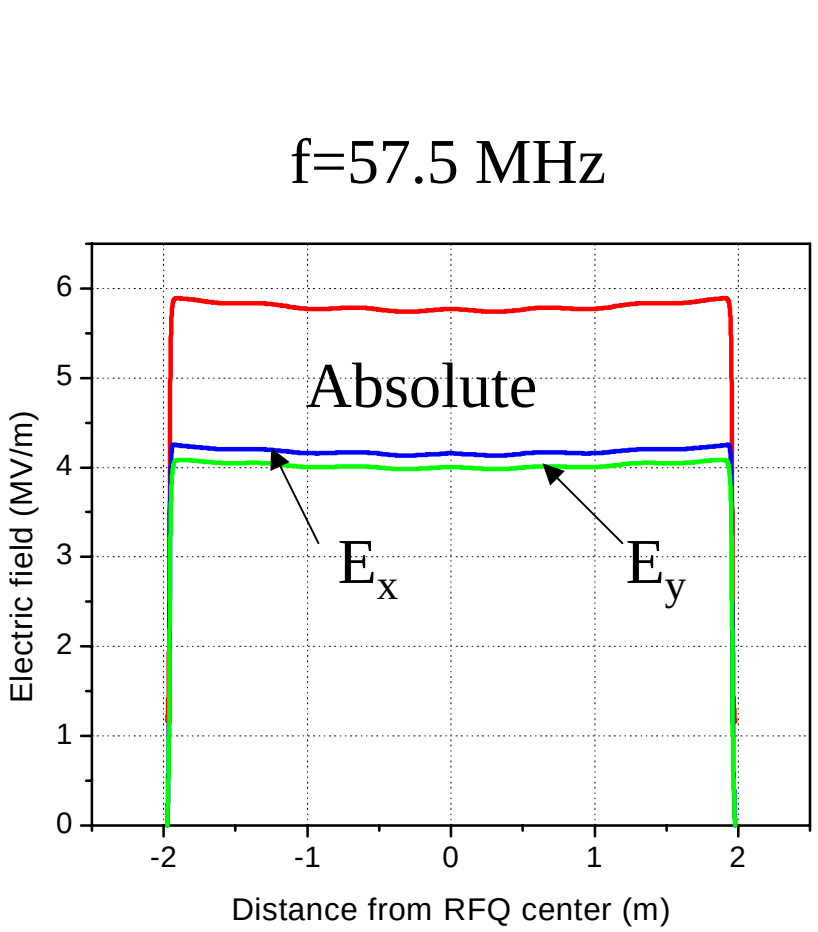

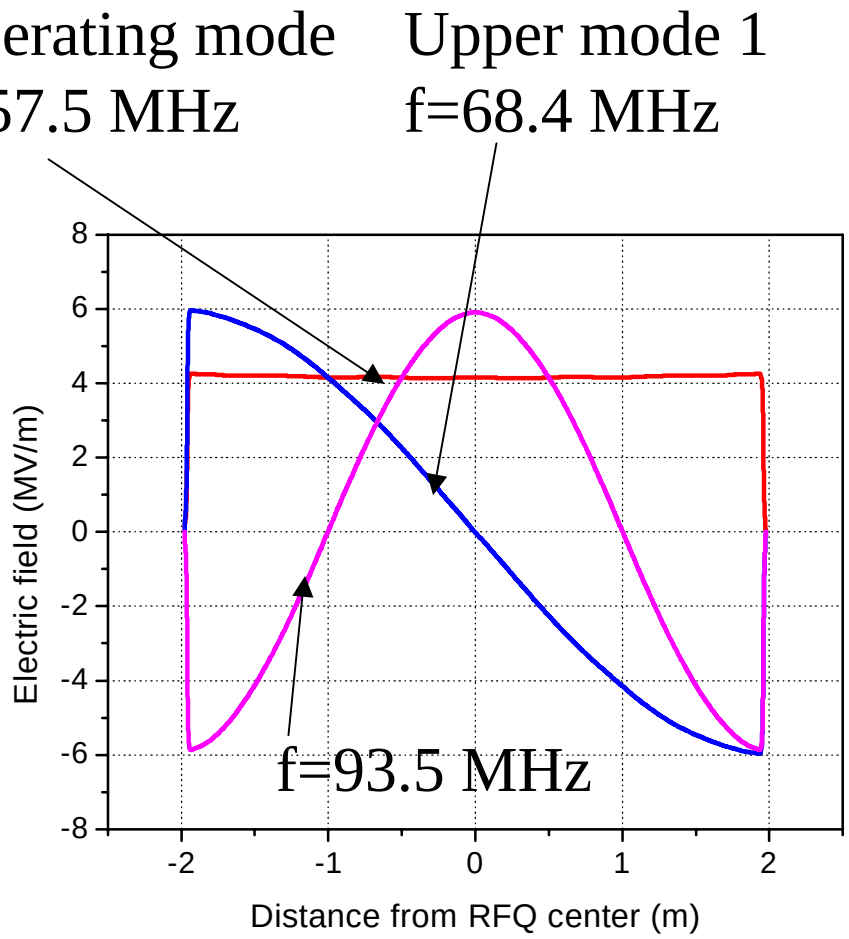

Cross Section of the Octagonal Resonator

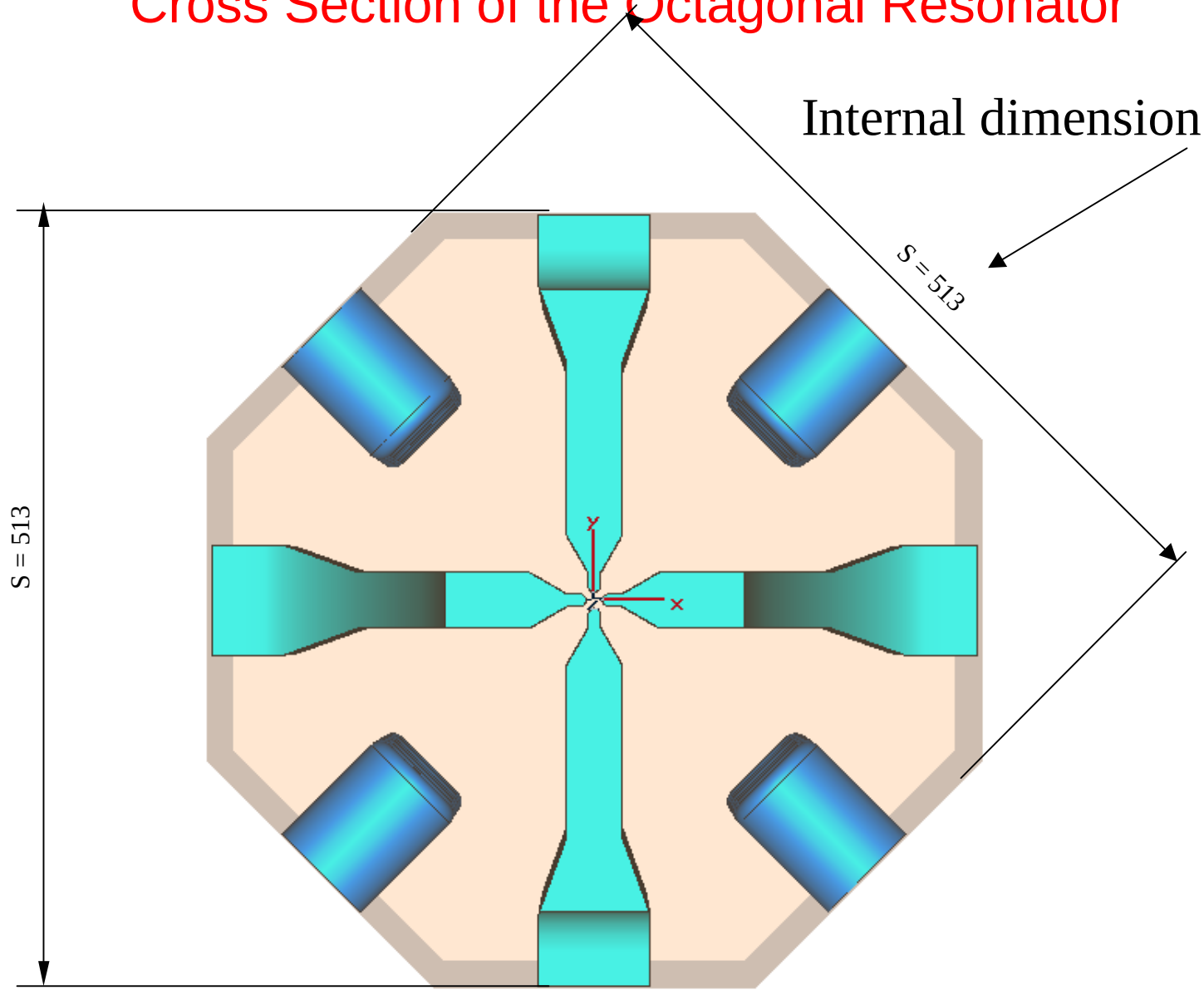

57.5 MHz Radio Frequency Quadrupole Accelerator

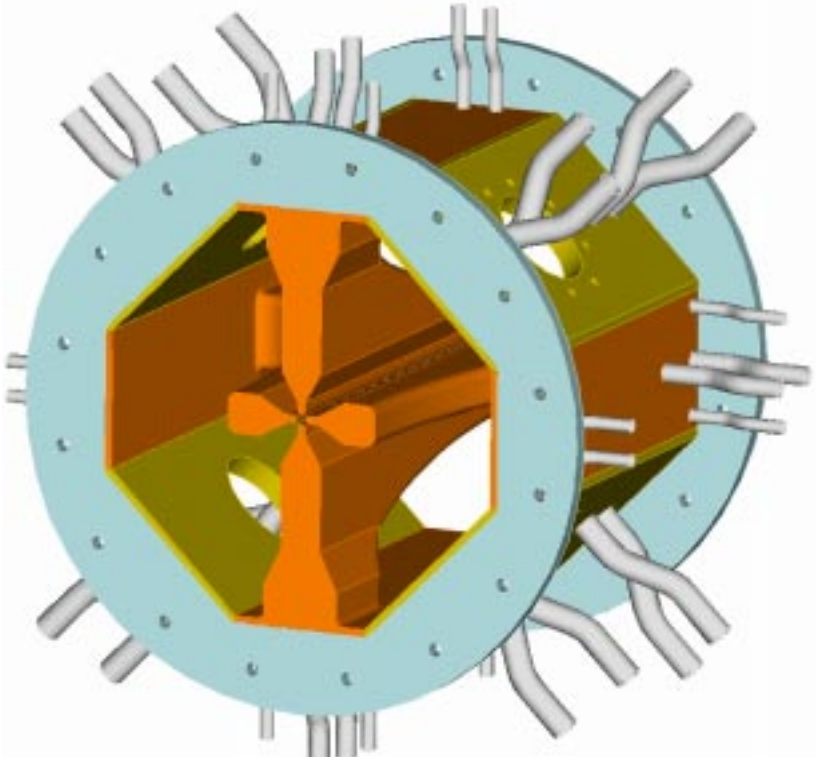

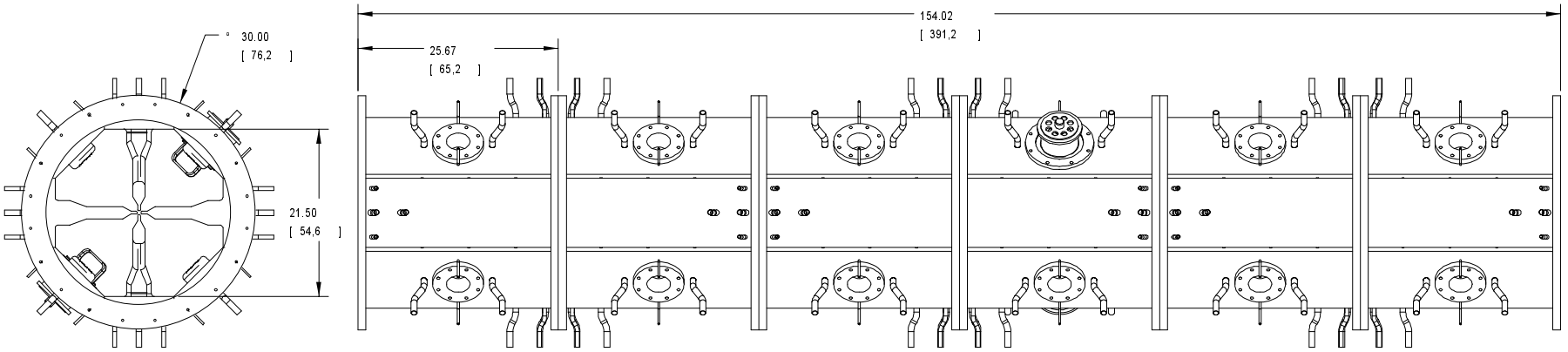

RF Induced Heat Flux

Heat flux distribution determined with ANSYS RF analysis, heat loads scaled to 8.0 kW per segment

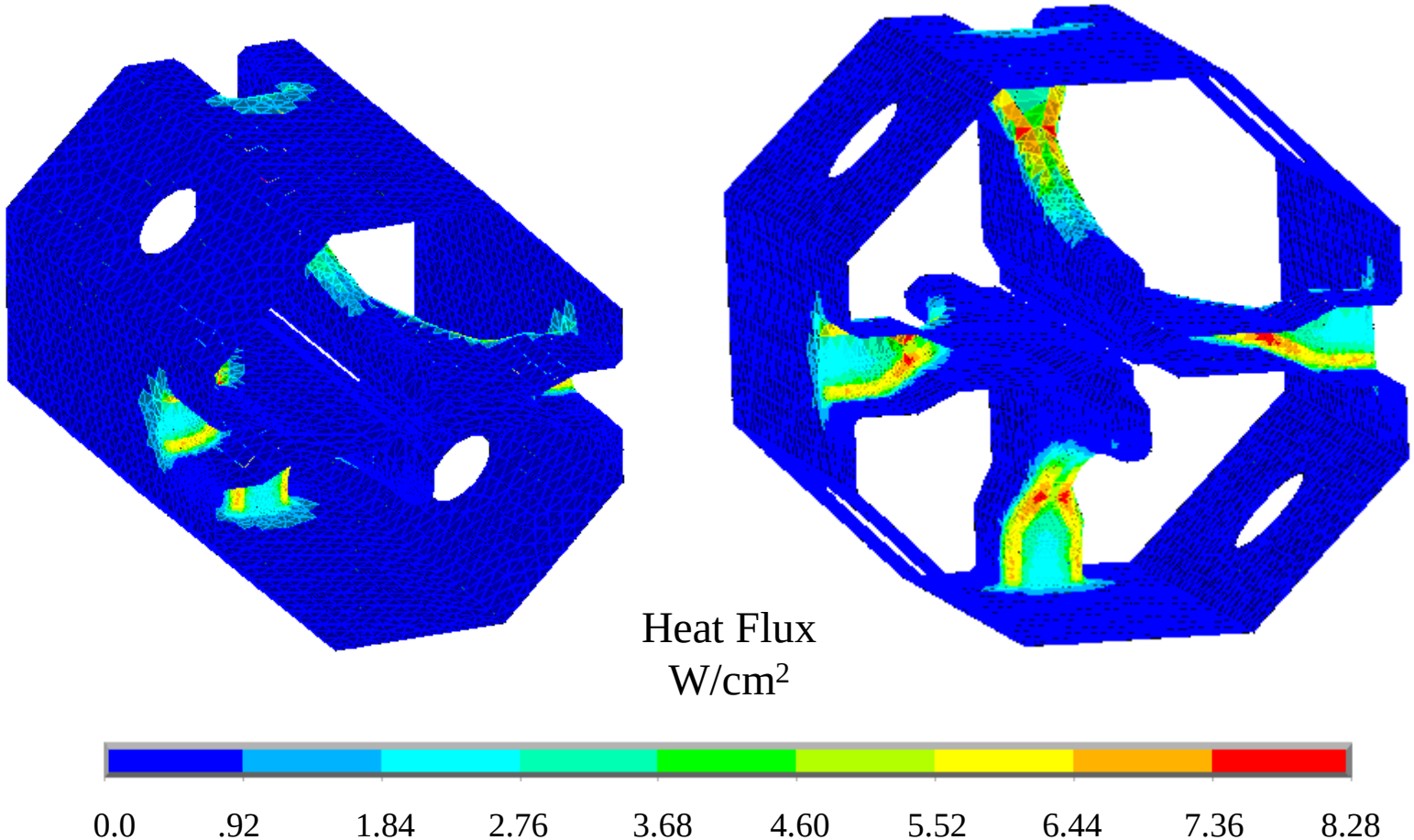

Radial displacements of Vanes at symmetry plane

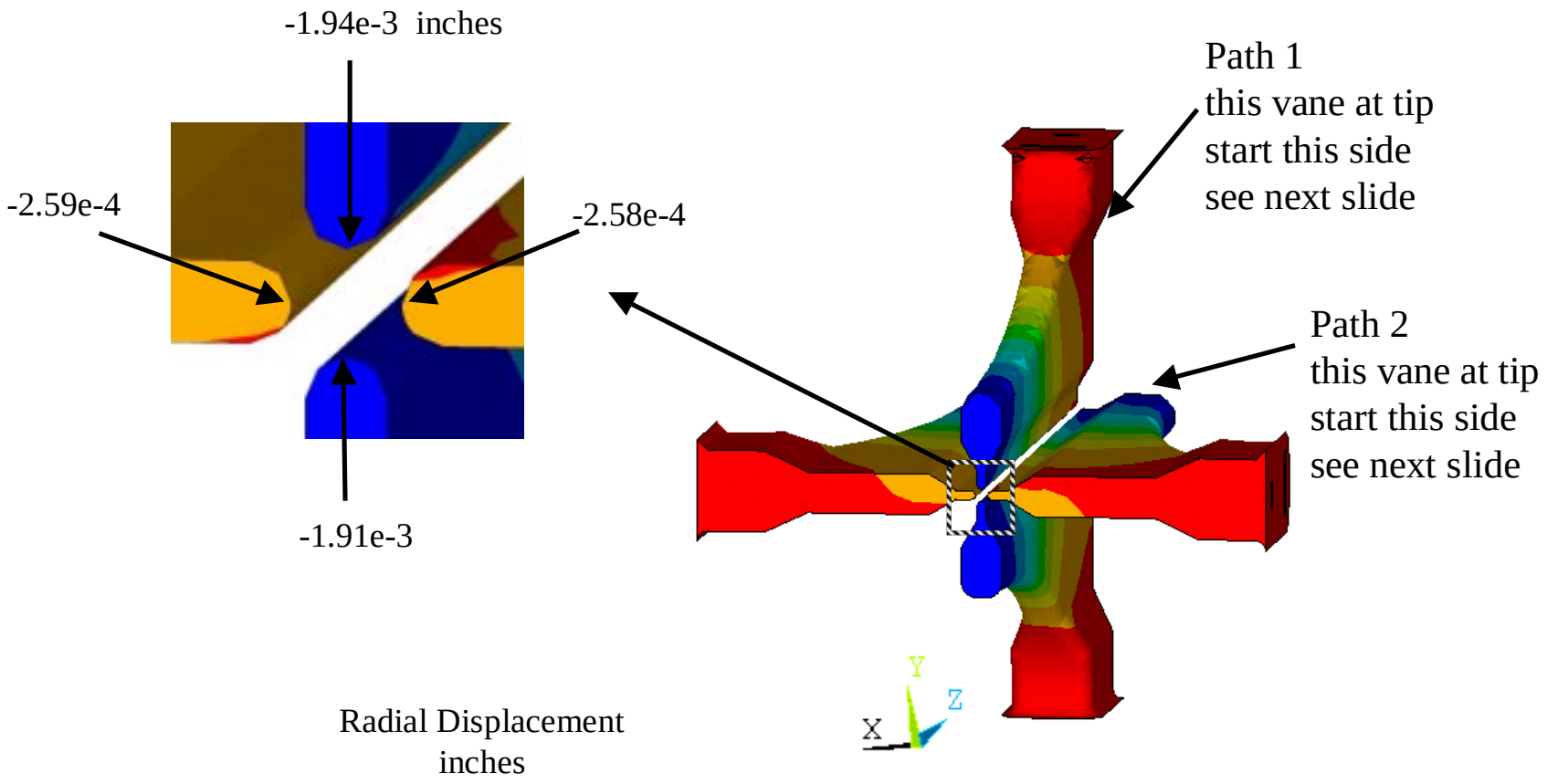

Characteristics of the RFQ resonator

- Modular structure. The brazing technique which is well established for 4-vane RFQs can be applied. Brazing provides the best electrical properties of rf structures;
- Small transverse dimensions for low frequencies;
- Large frequency separation of non-operating modes;
- Uniform field distribution along the z-axis;
- High shunt impedance (45 kW for 4 meter structure);
- Symmetric design guarantees low field perturbations due to possible thermal distortion, no dipole component of the fields in the aperture;
- Provides good mechanical stability of the construction together with precise alignment ability.

Electric potential in RFQ aperture

$$U(r,\vartheta,z)=\frac{U_l}{2}\left[F_0(r,\theta)+\sum_{n=1}^{\infty}F_{2n}(r,\vartheta)\cdot\cos 2nkz+\sum_{n=1}^{\infty}F_{2n-1}(r,\theta)\cdot\cos(2n-1)kz\right]$$

$$F_0(r,\theta)=\sum_{m=0}^{\infty}A_{0,2m+1}\left(\frac{r}{R_0}\right)^{2(2m+1)}\cdot\cos 2(2m+1)\theta$$

$$F_{2n}(r,\theta)=\sum_{m=0}^{\infty}A_{2n,2m+1}\cdot I_{2(2m+1)}(2nkr)\cdot\cos 2(2m+1)\theta$$

$$F_{2n-1}(r,\theta)=\sum_{m=0}^{\infty}A_{2n-1,2m}\cdot I_{4m}[(2n-1)kr]\cdot\cos 4m\vartheta$$

$$T=\frac{\pi}{4}\cdot A_{10}\quad\text{-}\quad\text{Accelerating efficiency}$$

$$K^2=\frac{eU_l}{4m_0c^2}\cdot\left(\frac{\lambda}{R_0}\right)^2 A_{01}\quad\text{-}\quad\text{Focusing efficiency}$$

Coupling of Longitudinal and Transverse Motions

$$\mathrm{H}(\Delta z, \Delta\beta) = \frac{c\Delta\beta^2}{2} + \frac{ZeU_0T}{\pi A W_0}\left(k\Delta z\cos\varphi_s - \mathrm{I}_0(kr)\sin(k\Delta z - \varphi_s)\right)$$

Separatrix of longitudinal oscillations calculated at the beginning of the RFQ (k=2.38)

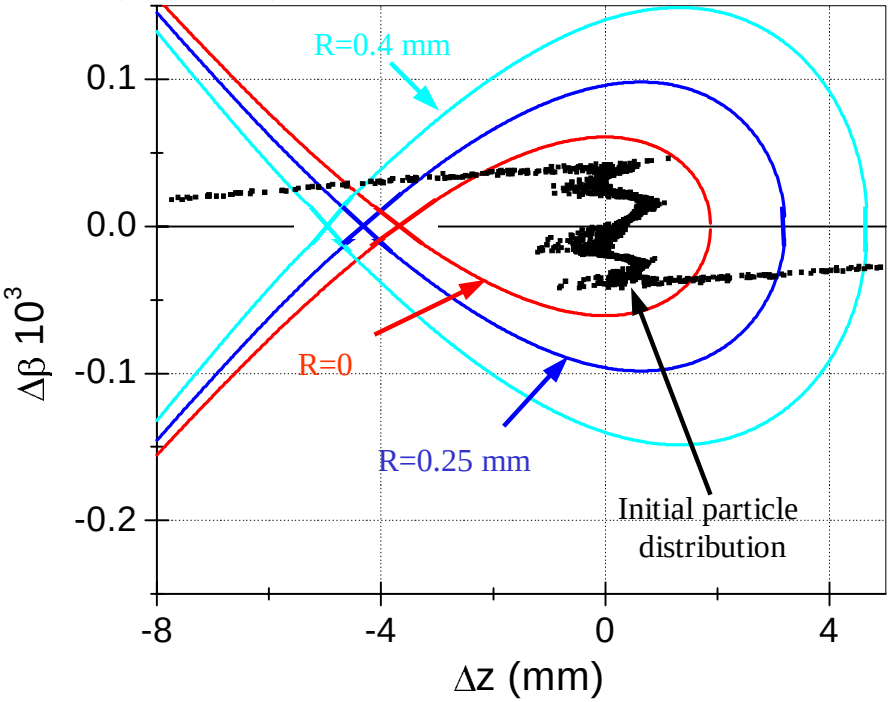

$$k = \frac{2\pi}{\beta\lambda}$$

$\Delta\beta = \beta - \beta_s$ Difference between particle velocity and synchronous value

$\Delta z = z - z_c$ The corresponding difference between longitudinal coordinates

Longitudinal emittances at the exit of RFQ

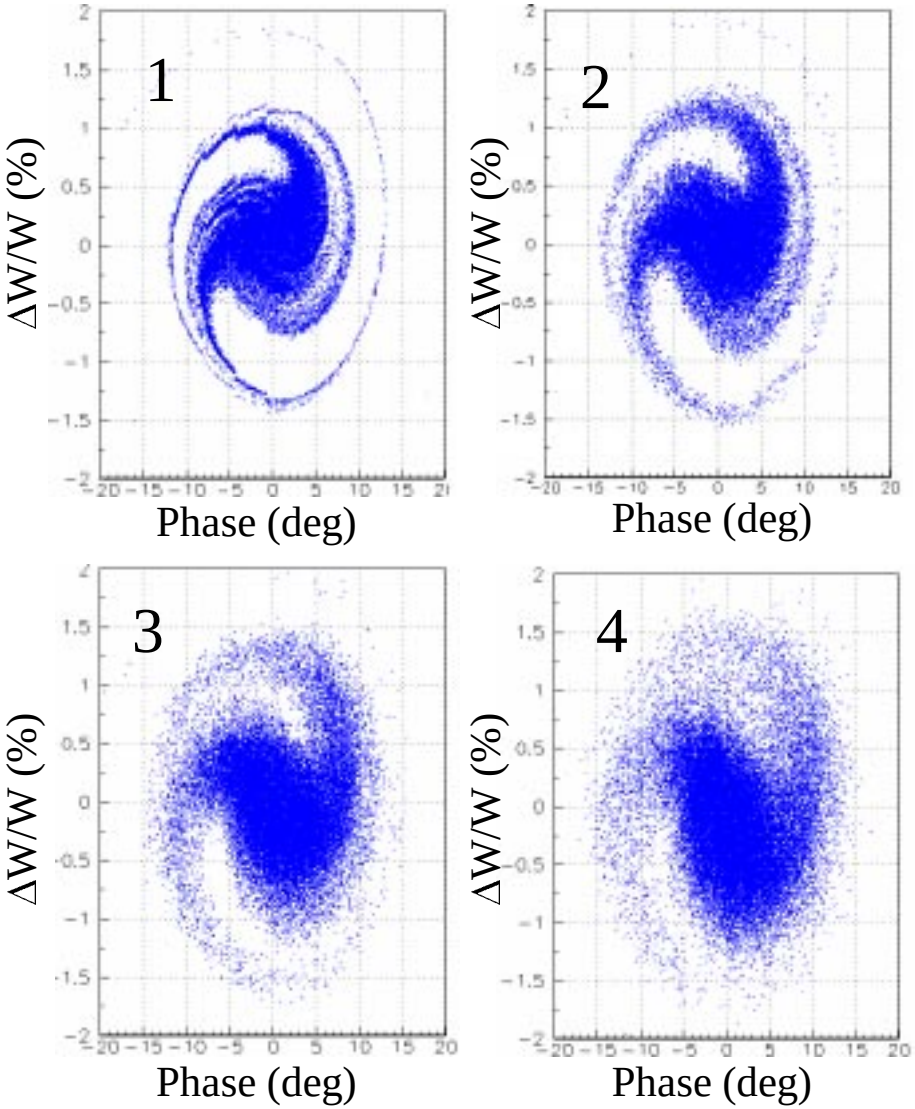

50000 particles are simulated

Longitudinal emittance
99.9 % of particles

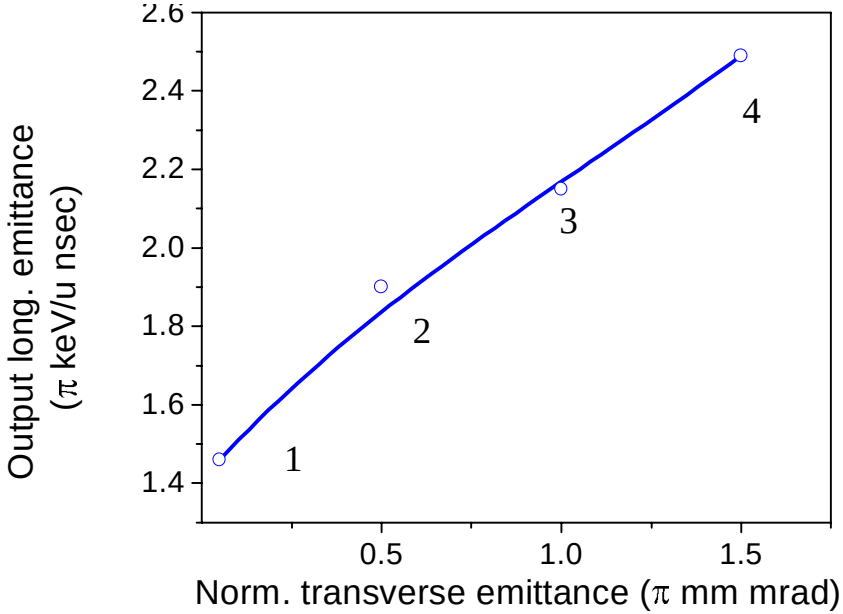

Transverse Emittances at the RFQ Exit

X plane

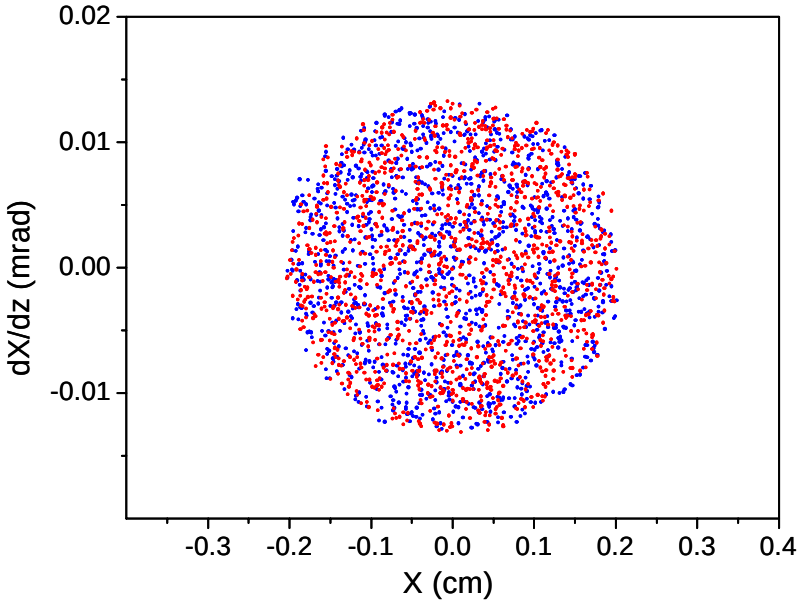

Y plane

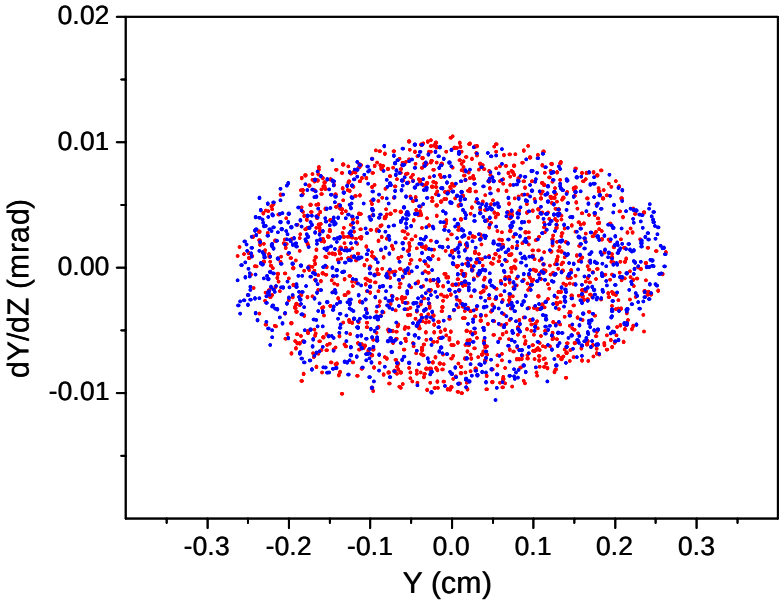

RIA Driver Linac

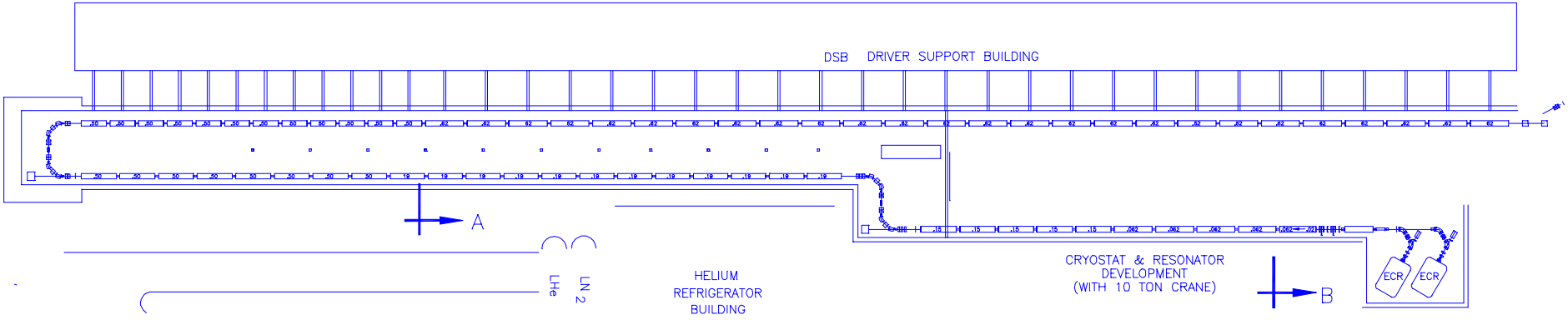

RESONATOR TYPE

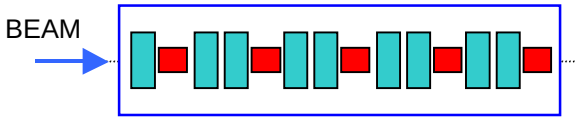

2-GAP QWR, β_G=0.062, f=57.5 MHz

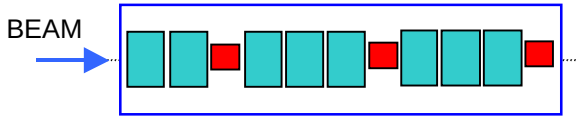

2-GAP QWR, β_G =0.15, f=115 MHz

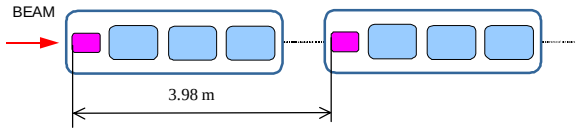

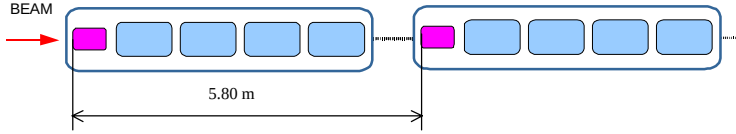

RESONATOR TYPE

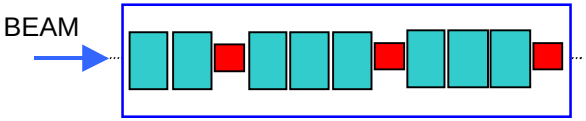

2-GAP HW, β_G=0.19, f=172.5 MHz

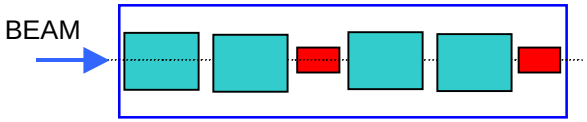

4-GAP SPOKE, β_G =0.5, f=345 MHz

4-GAP SPOKE, β_G =0.5, 0.62 f=345 MHz

Driver Linac

	Low β	Medium β	High β
Uranium beam energy, MeV/u	0.2-10.2	10.1-85.0	81.0-403.0
Surface field SRF cavities, MV/m	20	20	28.5
Frequency, MHz	57.5-115	172.5-345	805 (345)
Number of cryostats	10	20	46 (38)
Number of resonators	85	129	166 (140)
Number of focusing periods	42	52	46 (38)
Length of the focusing period, cm	113-177	177-250	400-580
Length, m	55	105	260 (197)

Some design solutions

- Multi-q beam acceleration.
- Low longitudinal emittance of two charge-state uranium beam.
- Inter-cryostat space will contain only vacuum valves and a small beam diagnostics box.
- Beam steering coils will be combined with the SC focusing solenoids and will not require an additional space along the beamline.
- Standard accelerating SRF cavities can be switched to the mode of a beam phase monitor in order to set up phases and amplitudes of the accelerating fields in the upstream cavities.
- Transverse matching between the cryostats is facilitated by the absence of the first SRF cavity in the very first focusing period of the cryostats.
- Long. matching between the cryostats is provided by the setting of phases in the SRF cavities.
- Beam energy at stripper locations is determined from the condition of lowest possible long. emittance of multi-q uranium beam.
- Triple spoke cavities vs elliptical.

Detailed BD simulations are necessary for cost-effective design of the accelerators

Simulation codes

- TRACE, TRANSPORT, COSY, GIOS;
- CST Microwave Studio; SIMION;
- DESRFQ, DYNAMION;
- RAYTRACE, TRACK.

TRACK:

- multiparticle simulation of multi-q ion beams in 6D phase space;
- 3D electromagnetic fields from MWS in rectangular mesh;
- Fringing fields of magnets and multipoles as in RAYTRACE code;
- Realistic fields in solenoids;
- Integration of equations of motion by 4^{th} order Runge-Kutta method;
- Misalignments and random errors are included.

Beam envelopes along the driver linac

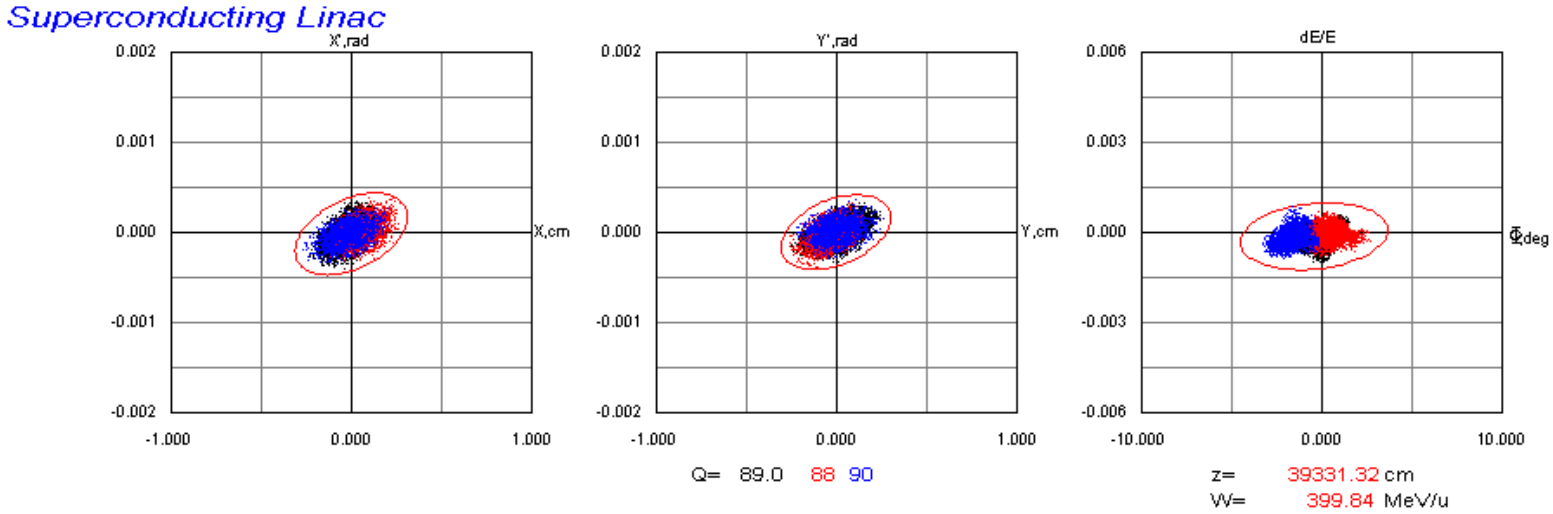

Parametric resonance

The condition for a n-th order parametric resonances of transverse motion in a smooth approximation

$$\mu_t = \frac{n}{2}\mu_l$$

Resonance width

$$a_n \Delta_s < \mu_t^2 < b_n \Delta_s$$

Longitudinal phase advance

$$\mu_l = 2\sqrt{\Delta_s}$$

Defocusing factor

$$\Delta_s = \frac{\pi}{2}\frac{q}{A}\frac{1}{(\beta_s\gamma_s)^3}\frac{S_f^2}{\lambda}\frac{eE_m \sin\varphi_s}{m_u c^2}$$

$n=1$ and $\varphi_s=30°$: $a_1 \approx 0,\ b_1 \approx 1.79$

$n=2$ $a_2 \approx 3.93,\ b_2 \approx 4.31.$

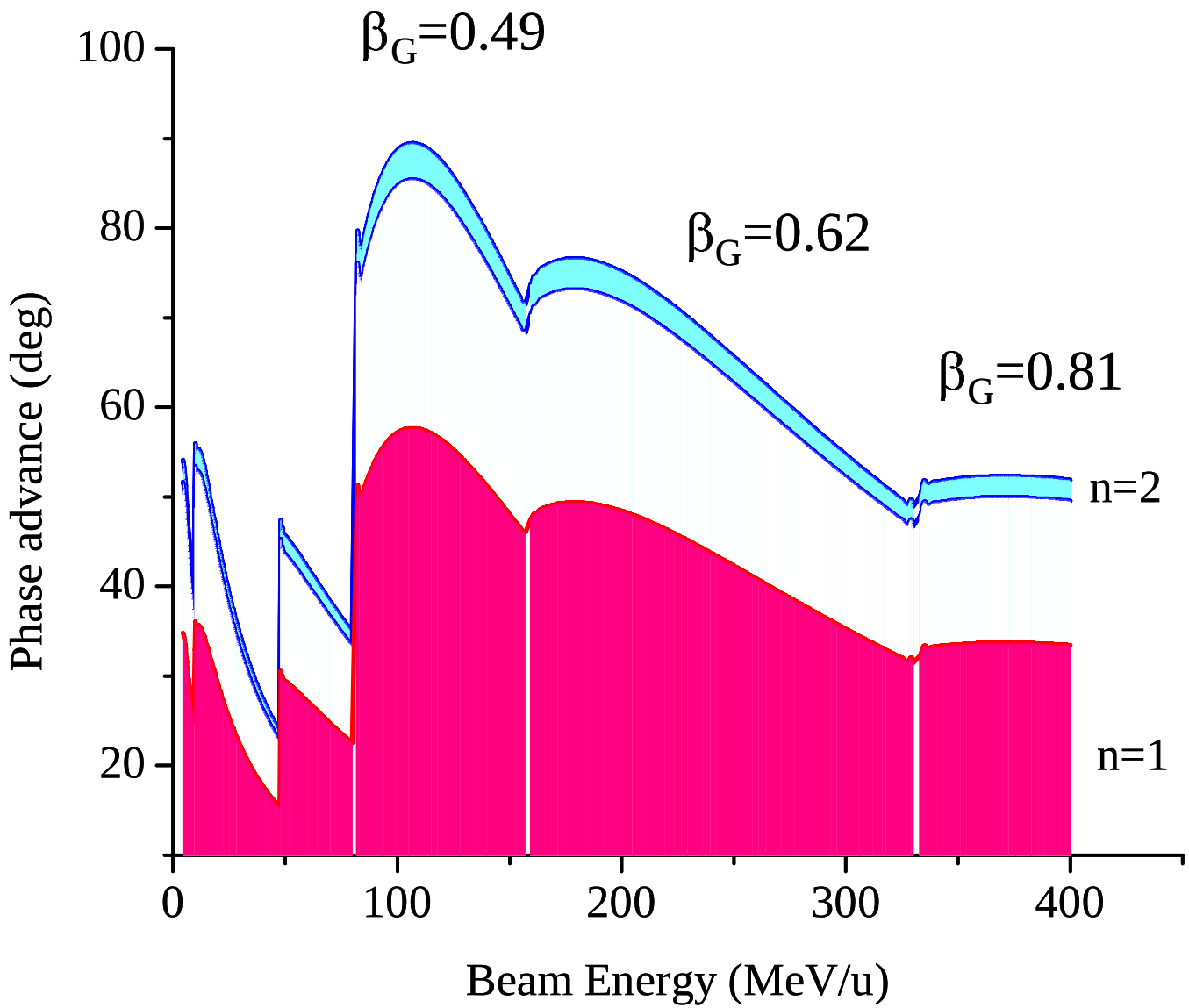
β_G=0.49
β_G=0.62
β_G=0.81
n=2
n=1
Phase advance (deg)
Beam Energy (MeV/u)
100
80
60
40
20
0
100
200
300
400

DTL section, 172. 5 MHz

RMS emittance,
μ_t=30°

W_{in}=10 MeV/u

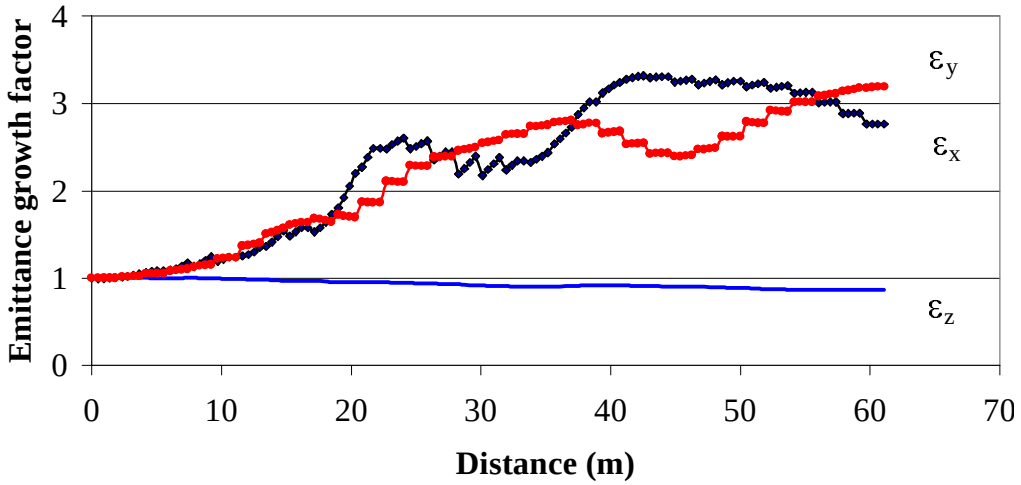

Emittance containing
99.9% of the particles

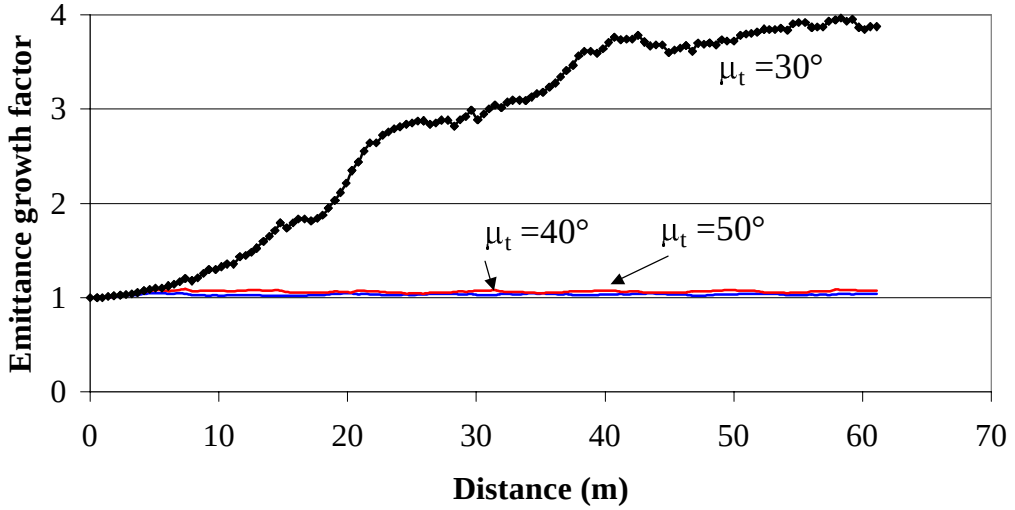

Emittance evolution along the ECL linac for 4-cavity and 3-cavity lattices

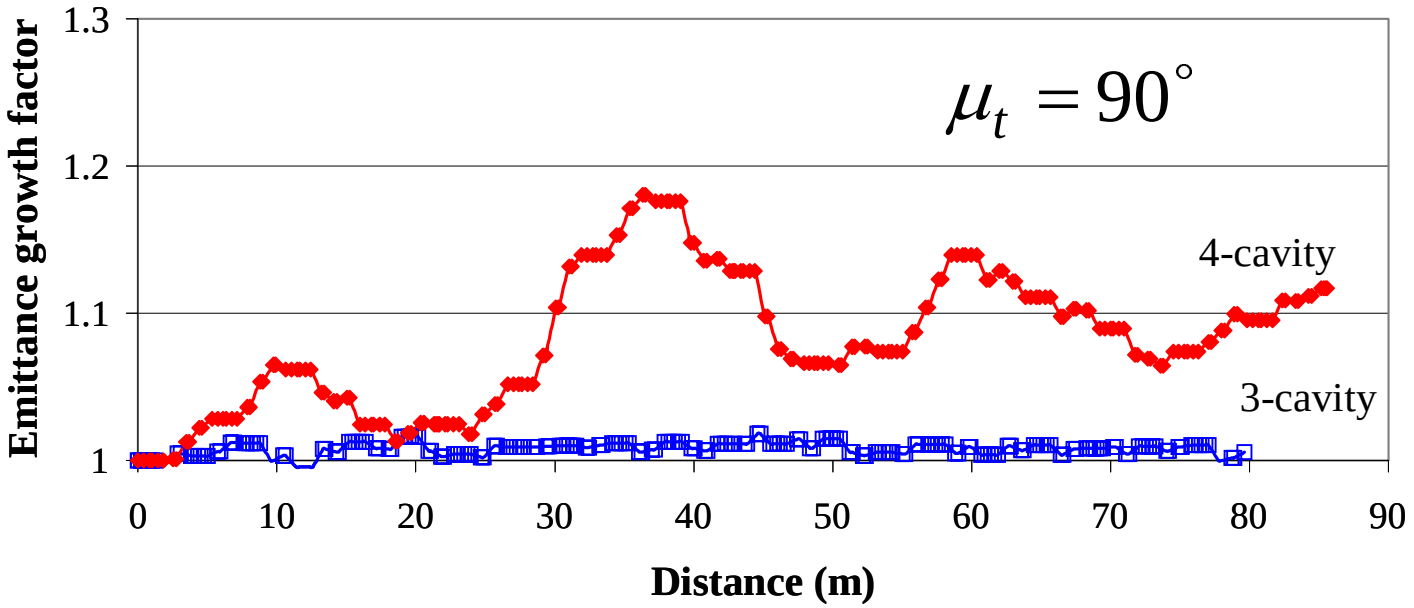

Proposed lattice
for the first section
of the ECL (β_G=0.49)

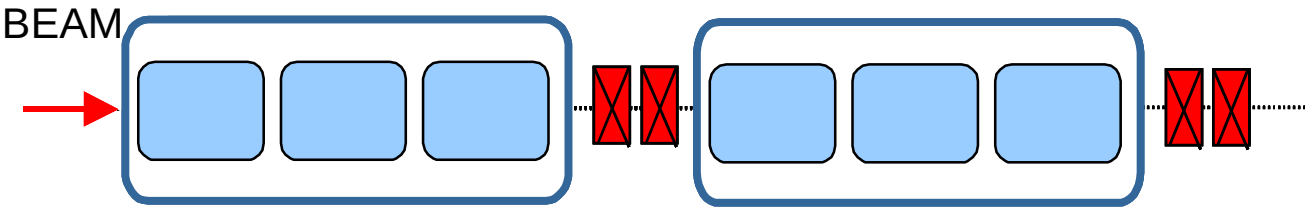

Beam steering in QWR*

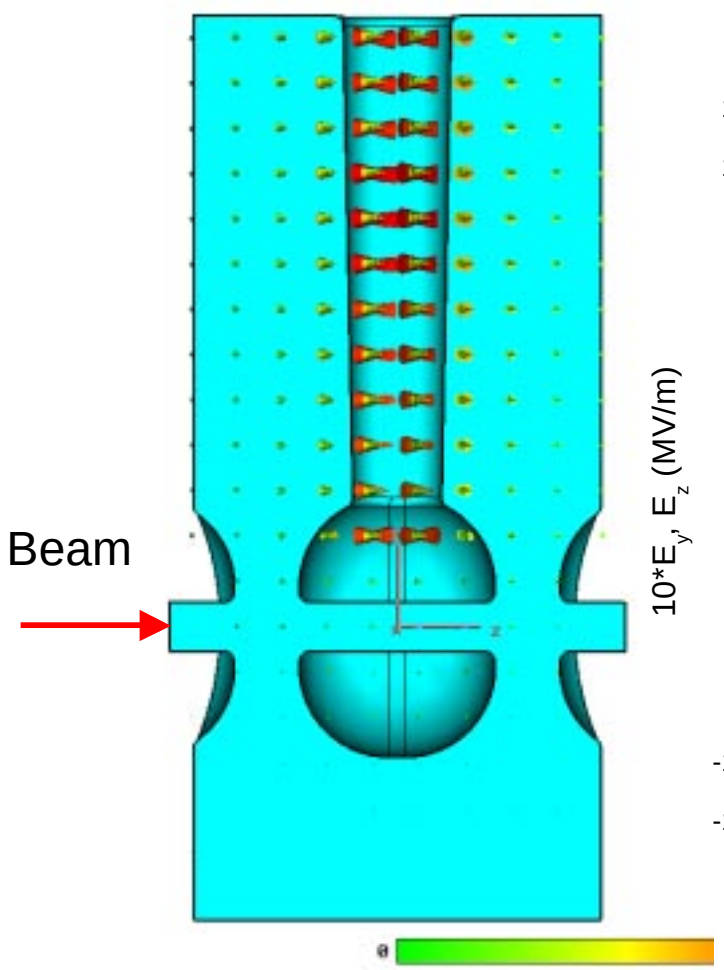

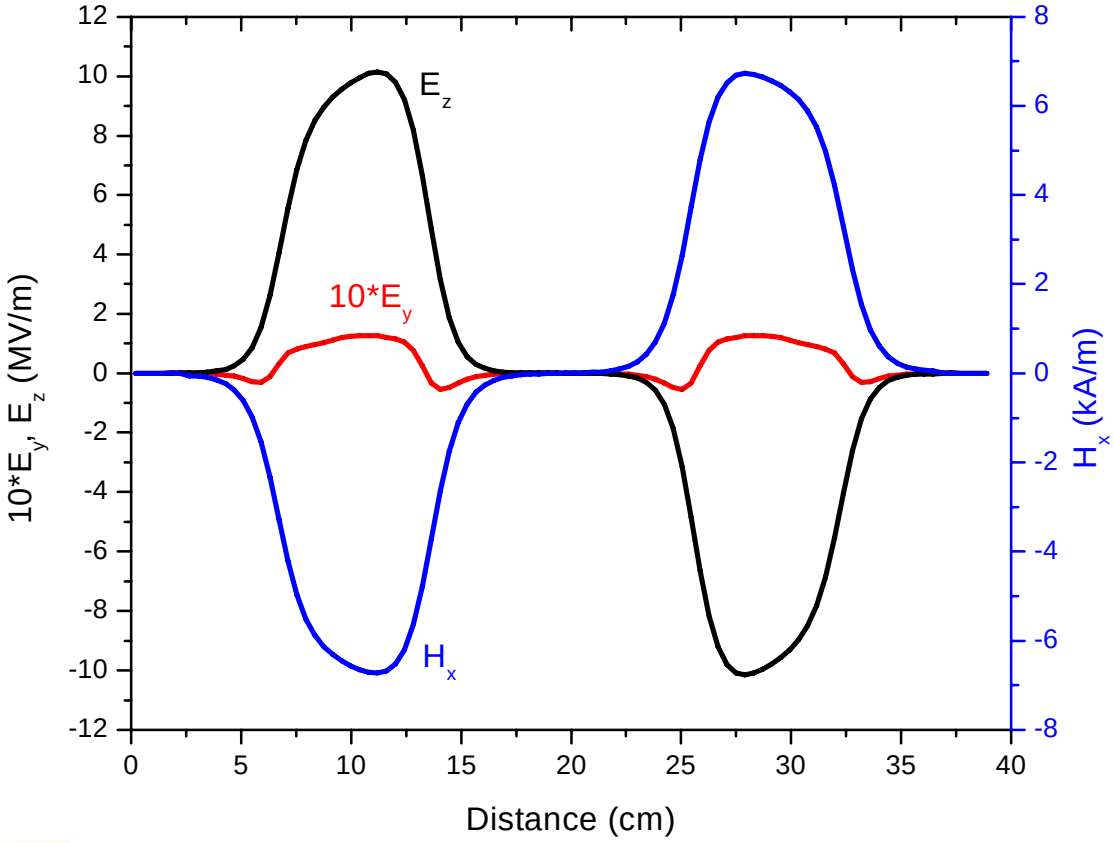

*A. Facco&V. Zviagintsev PAC91, N. Kakutani et al in EPAC98

Beam center deflection angles in QWR

$$\alpha_{TOT} = \alpha_{Ed} + \alpha_{Ef} + \alpha_{H}$$

$$\alpha_{Ed} = -C_0 \int_{-L/2}^{L/2} E_{yd}(z) \sin(kz + \varphi) dz$$

$$\alpha_{Ef} = \frac{y_0 C_0}{2} \int_{-L/2}^{L/2} \frac{\partial E_z(z)}{\partial z} \sin(kz + \varphi) dz$$

$$\alpha_{H} = \beta c \mu_0 C_0 \int_{-L/2}^{L/2} H_x(z) \cos(kz + \varphi) dz$$

Compensation of the beam-steering effect

(1) By cavity displacement in vertical plane: useful for heavy ions, accepted as a baseline design for the ISAC-II

(2) By reshaping of the drift tubes: universal far all regimes.

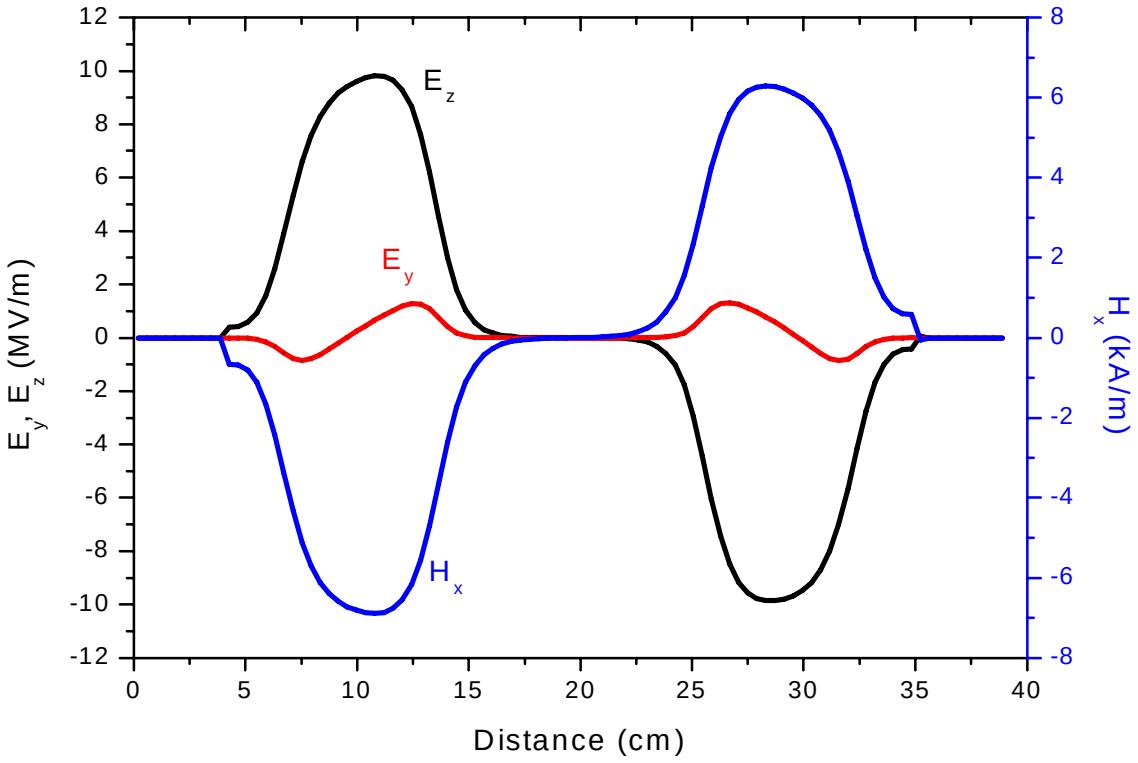

Beam steering in QWR

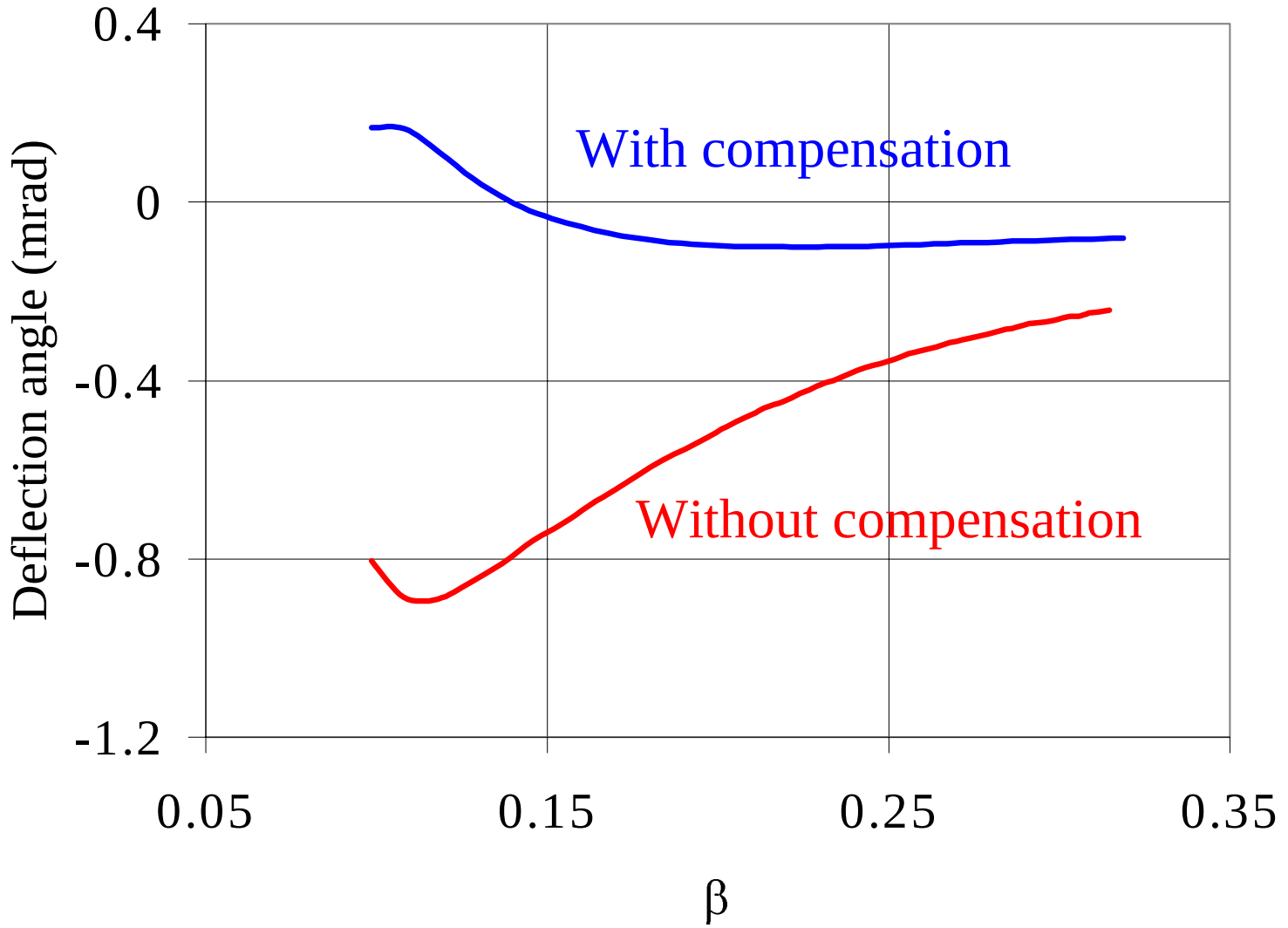

Defocusing field asymmetry in DT SRF cavities*

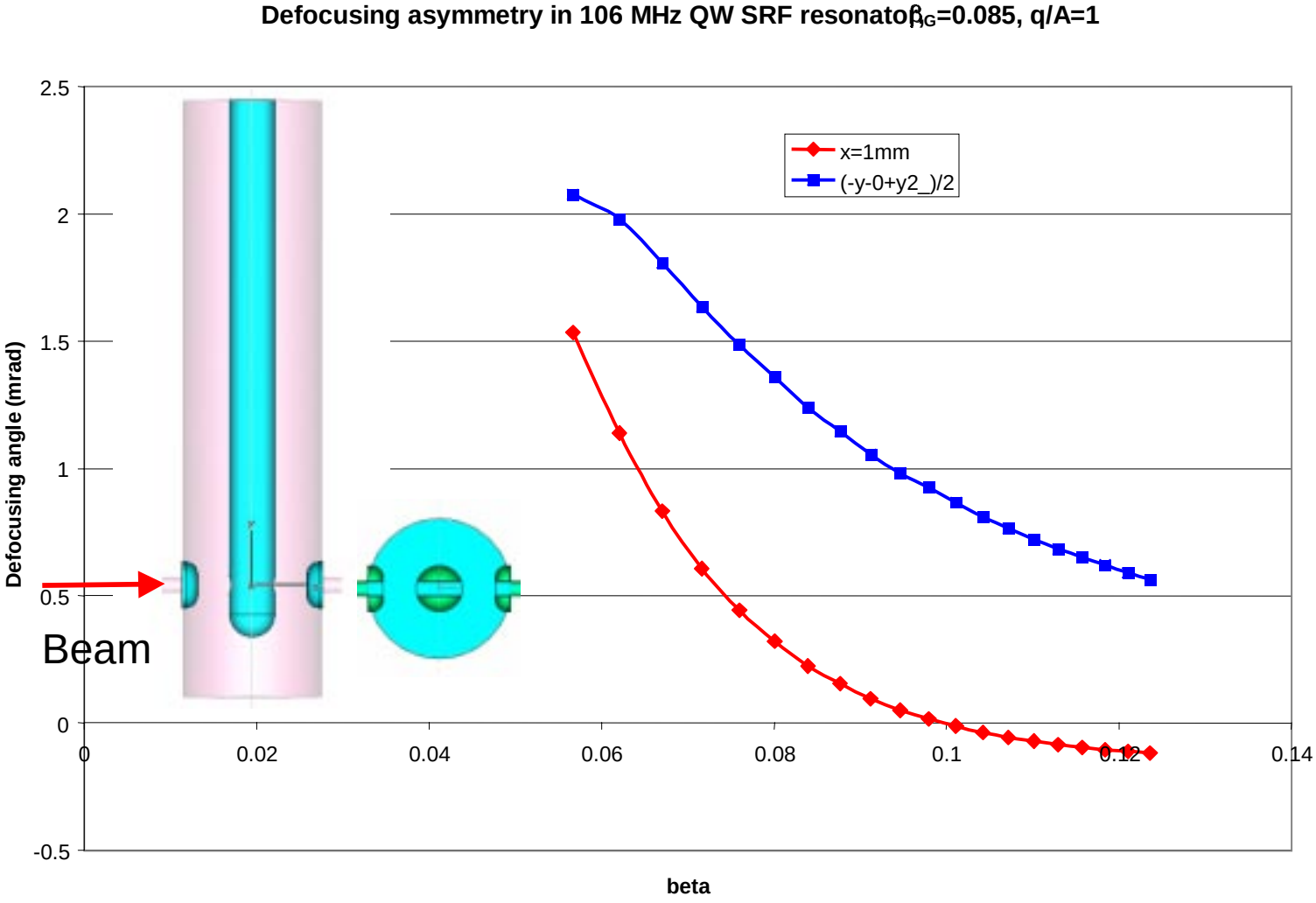

*Details will be presented in EPAC2002 by B. Laxdal, P.N. Ostroumov and M. Pasini.

Defocusing field symmetry in DT SRF cavities

Defocusing angles in 57.5 MHz QW SRF resonator, β_G=0.062, q/A=1

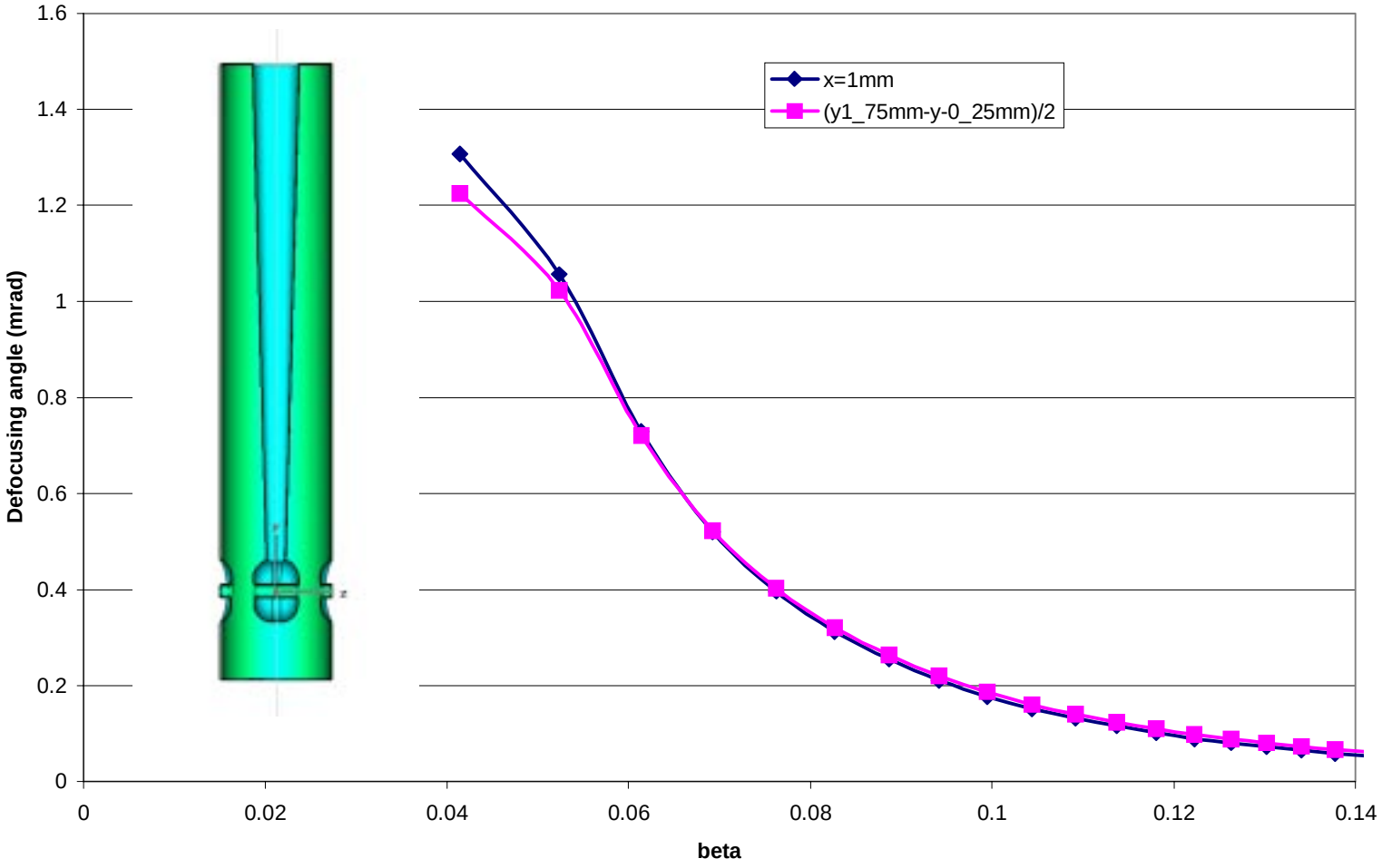

QUADRUPOLE COMPONENT OF TRANSVERSE RF ELECTRIC FIELD

Harmonic analysis of the electric field along the axis of HWR in cylindrical coordinates

$$V = -A_{20} r^2 - A_{22} r^2 \cos(2\phi)$$

$$E_r = -\frac{\partial V}{\partial r} = 2A_{20}\, r + 2A_{20}\, r\, \cos(2\phi)$$

$$E_\phi = -\frac{1}{r}\frac{\partial V}{\partial r} = -2A_{22}\, r\, \sin(2\phi)$$

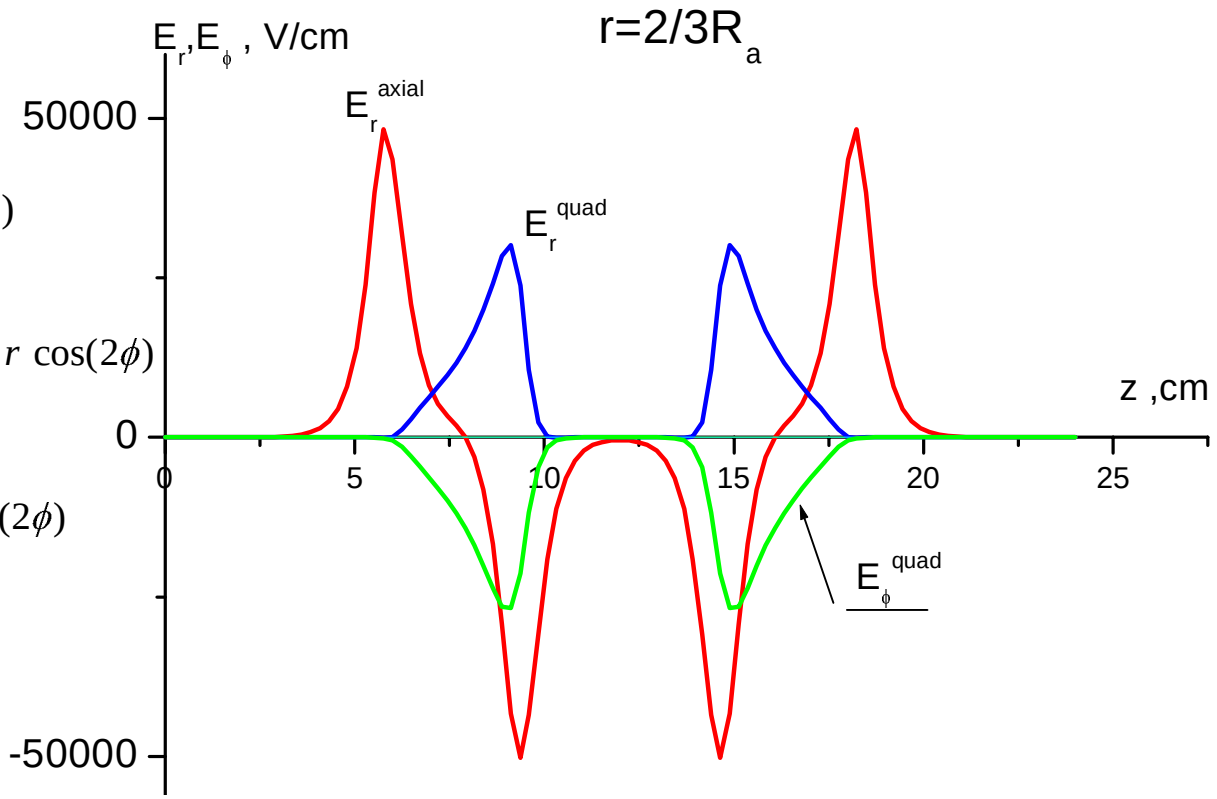

Input beam, 2 charge states:

100% of particles

2.4 π keV/u-nsec

0.5 π mm-mrad

Longitudinal phase space, W=199 keV/u

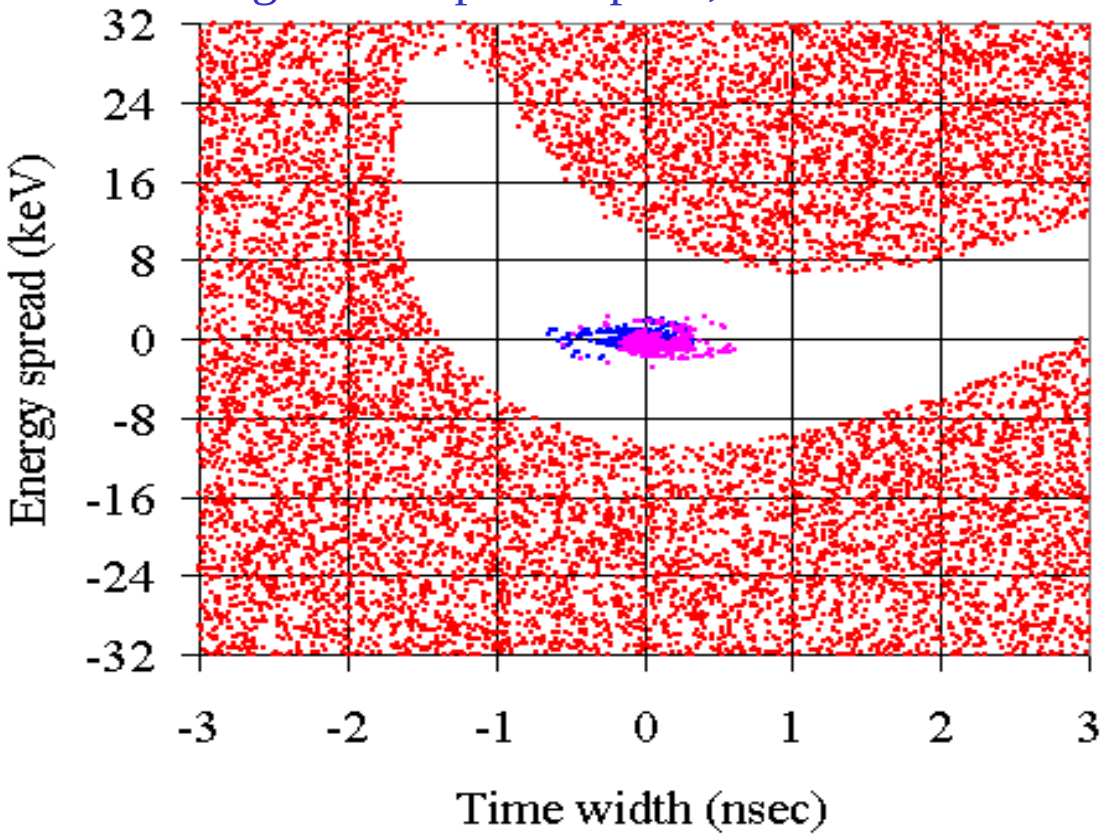

Beam envelopes along the prestripper section

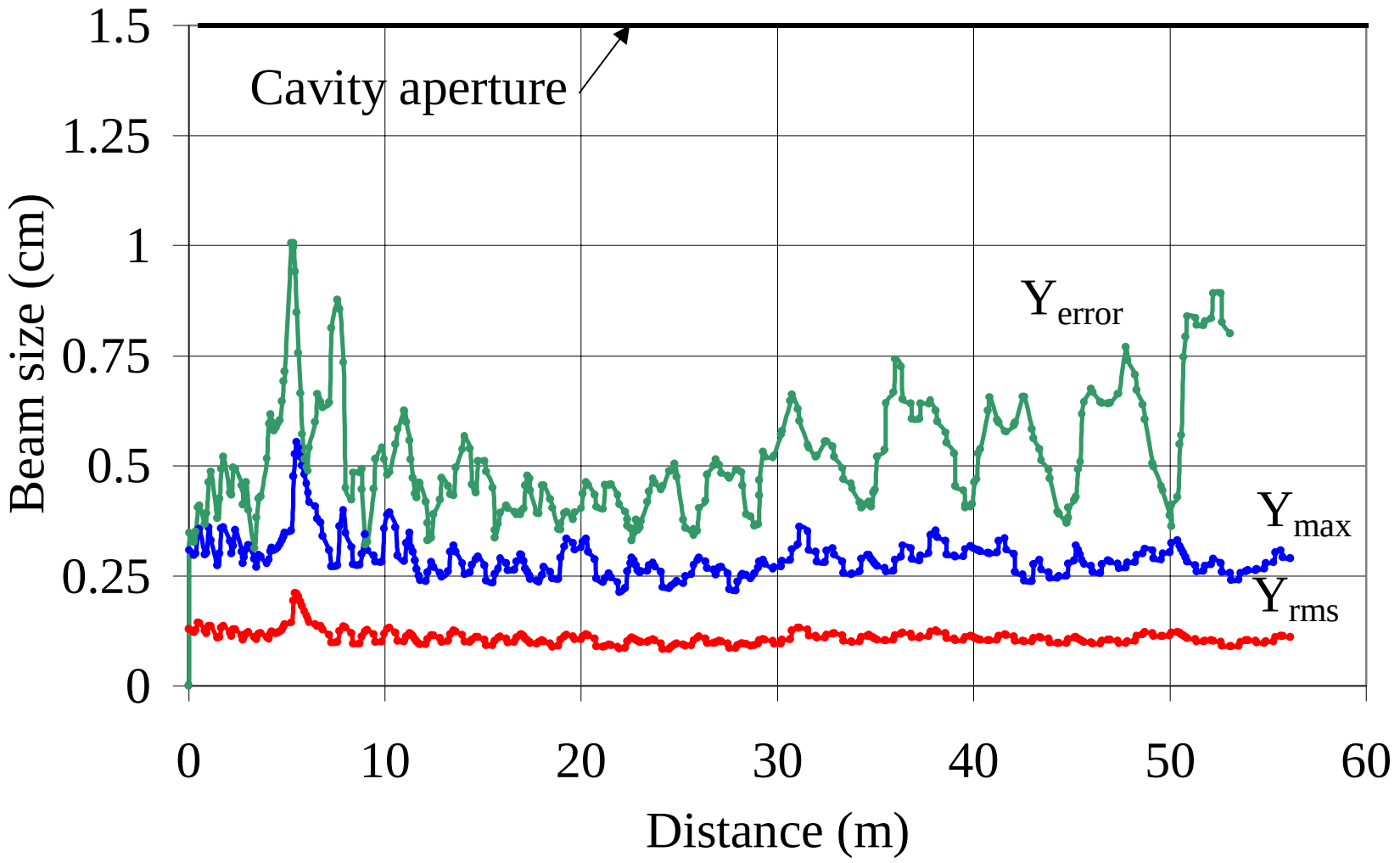

RMS emittance growth of two-charge state uranium beam in the misaligned focusing channel of low-β linac with the steering correction.

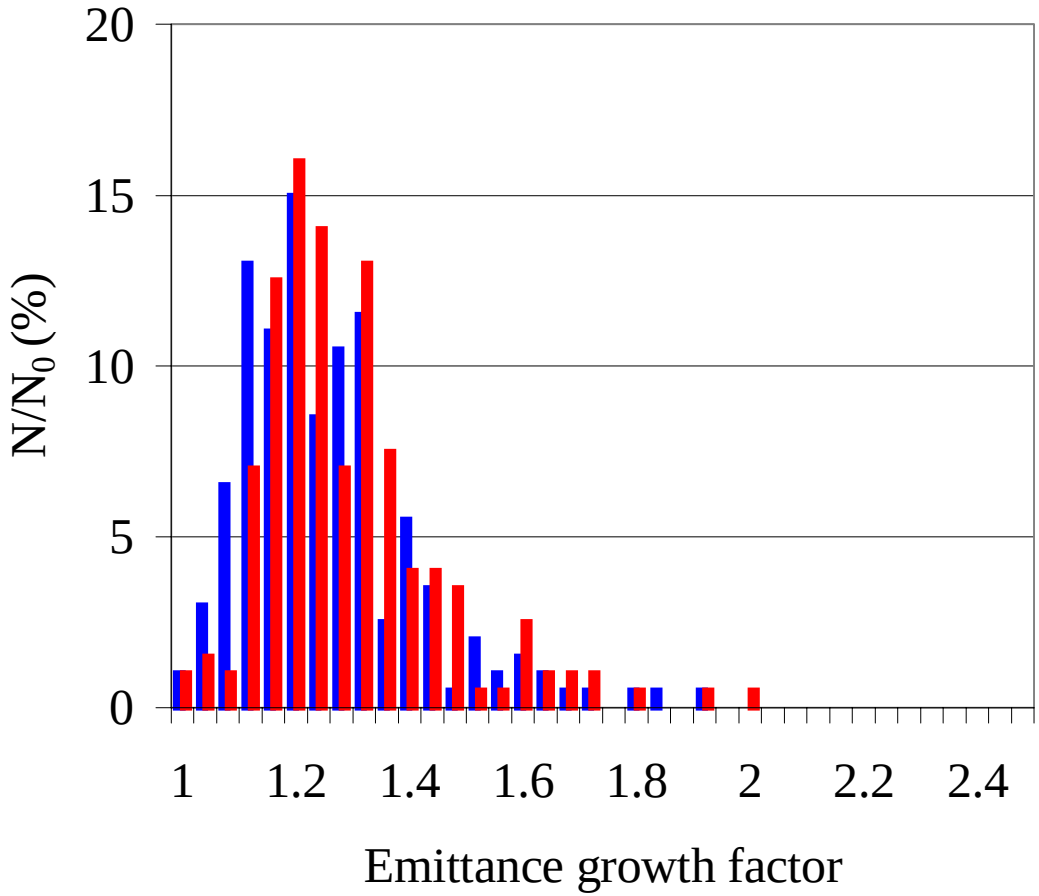

Focusing by SC solenoids:

- proven technology with SC resonators;
- multi-q beam is less sensitive to mismatched conditions;
- the fringing fields can be suppressed by bucking coils;
- alignment of the solenoids should be easier;
- beam is less sensitive to solenoid misalignments.

Compact 9 Tesla SC Magnet Assembly

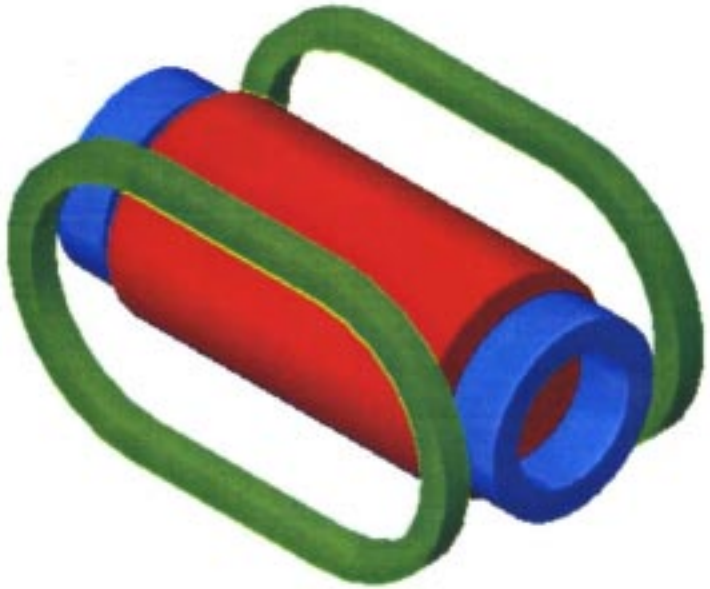

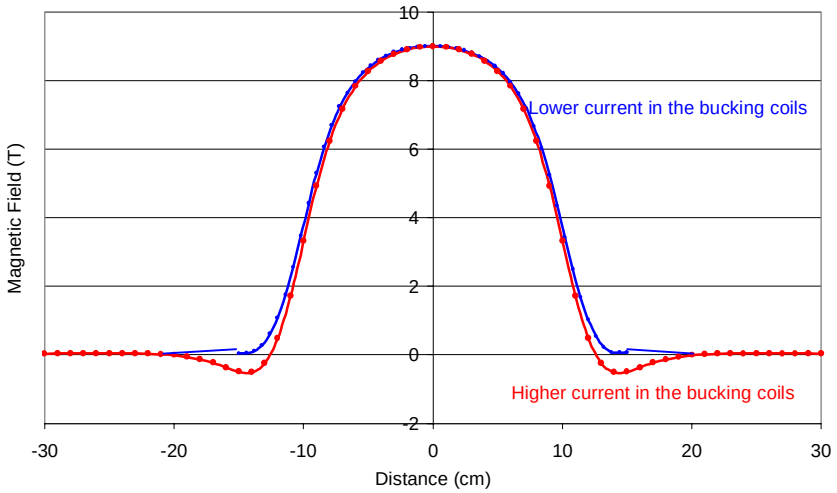

Longitudinal emittance along the prestripper linac

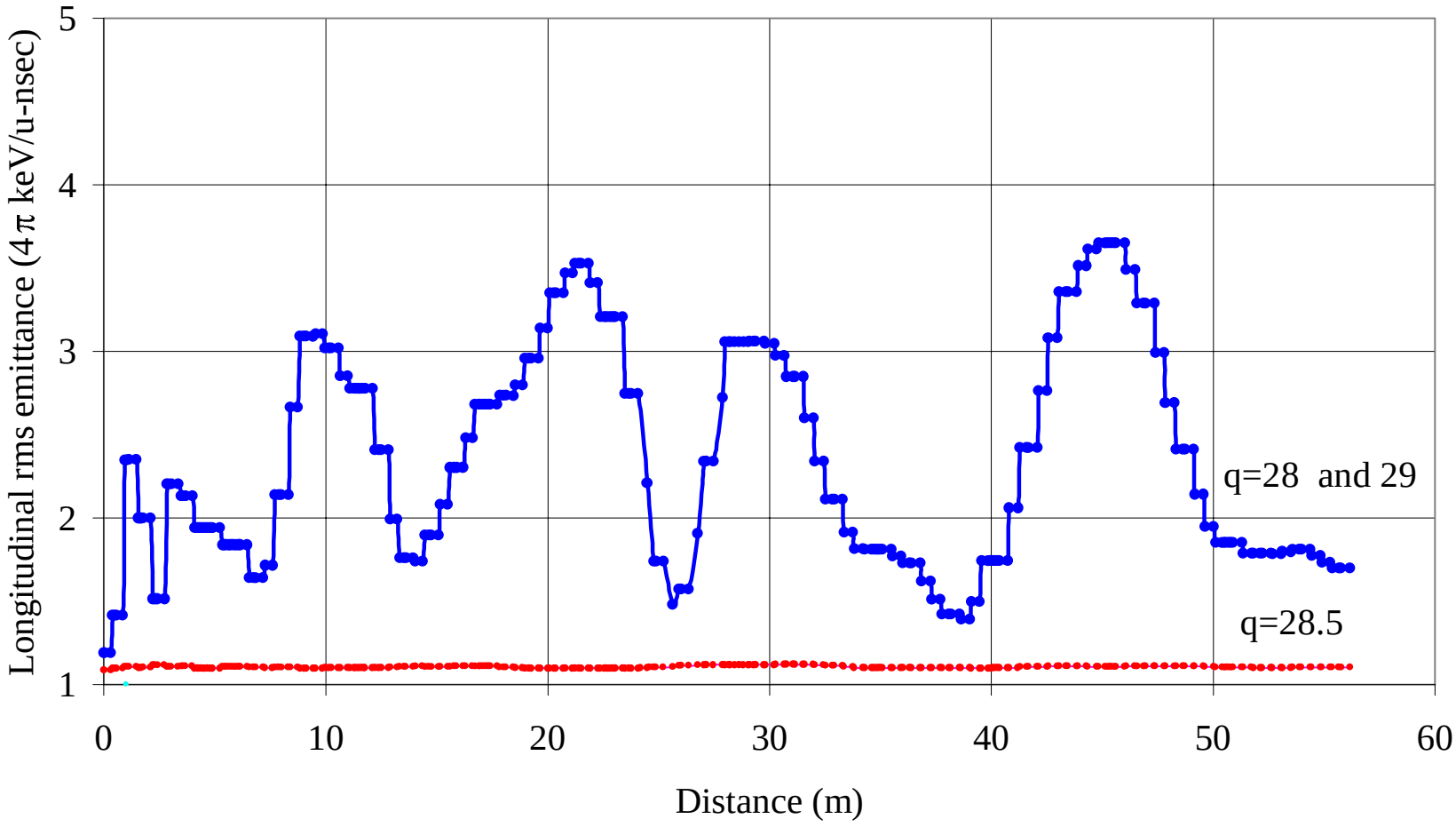

Particle trajectories in the longitudinal phase space

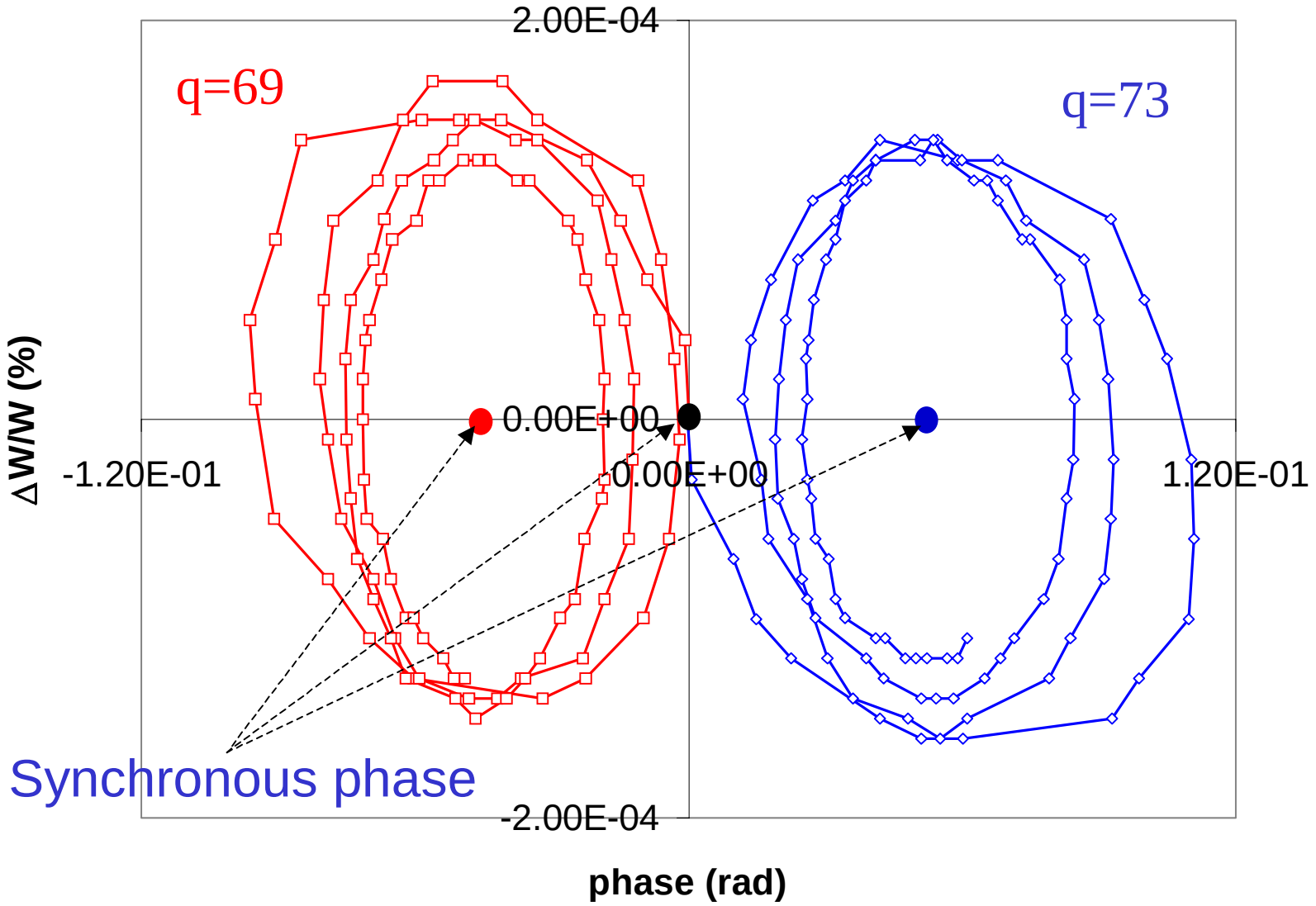

Longitudinal phase space, W=9.4 MeV/u

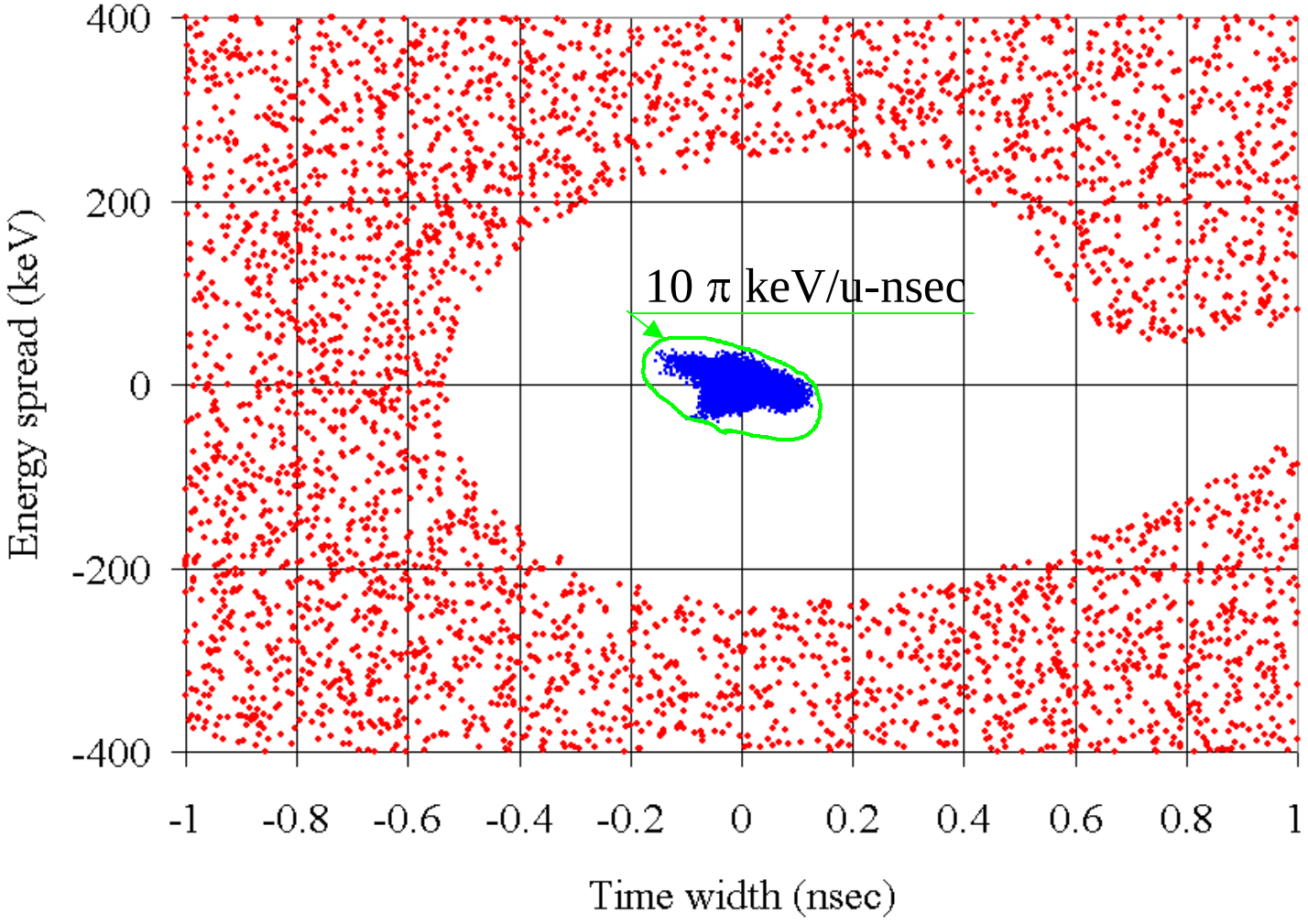

Phase space plots of 5 charge state uranium beam at the location of second stripper linac 85 MeV/u

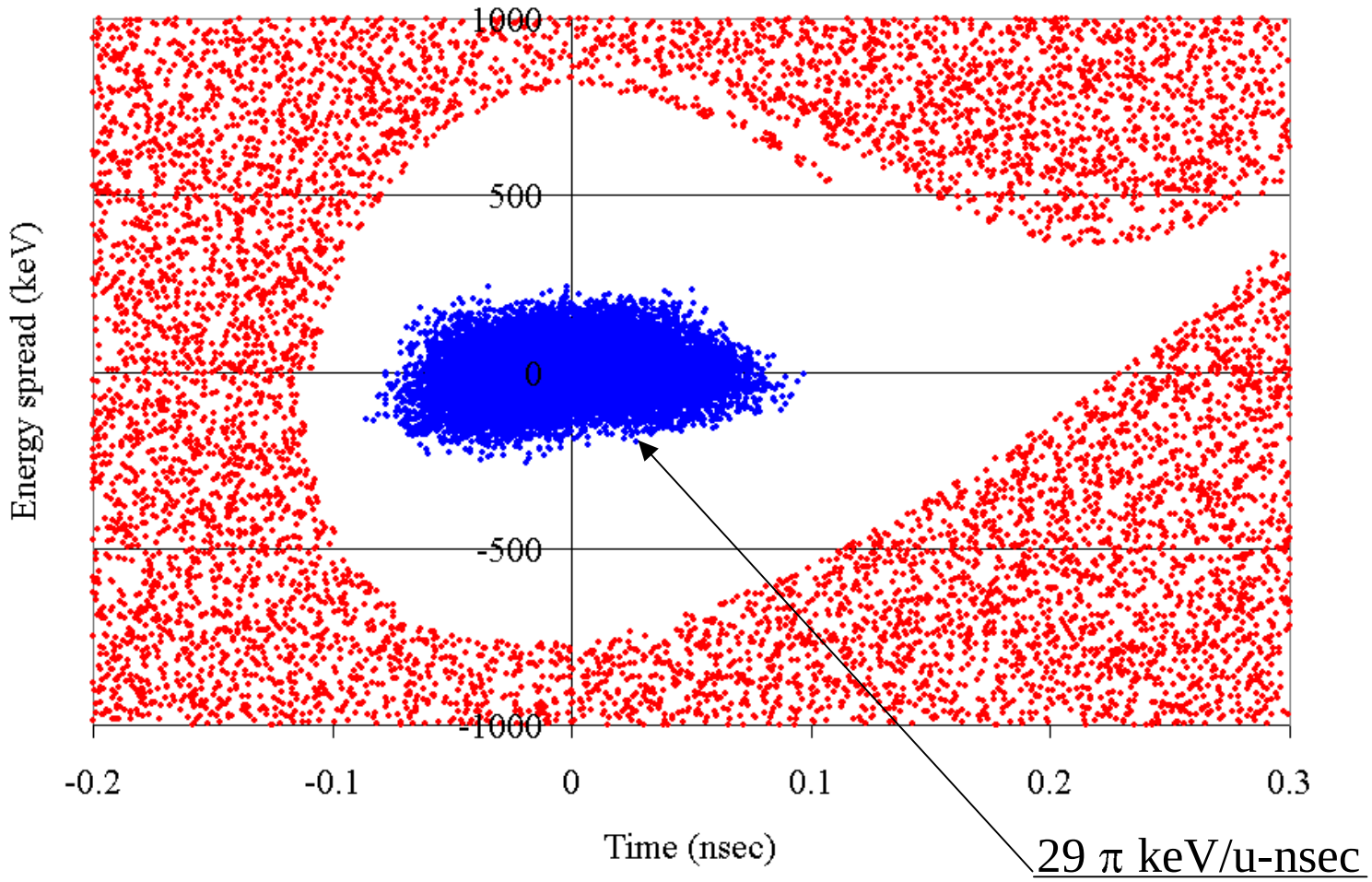

Phase space plots of four charge state uranium beam at the exit of the driver linac. Includes all rf field errors and multiplicity of charge states throughout whole SC Linac

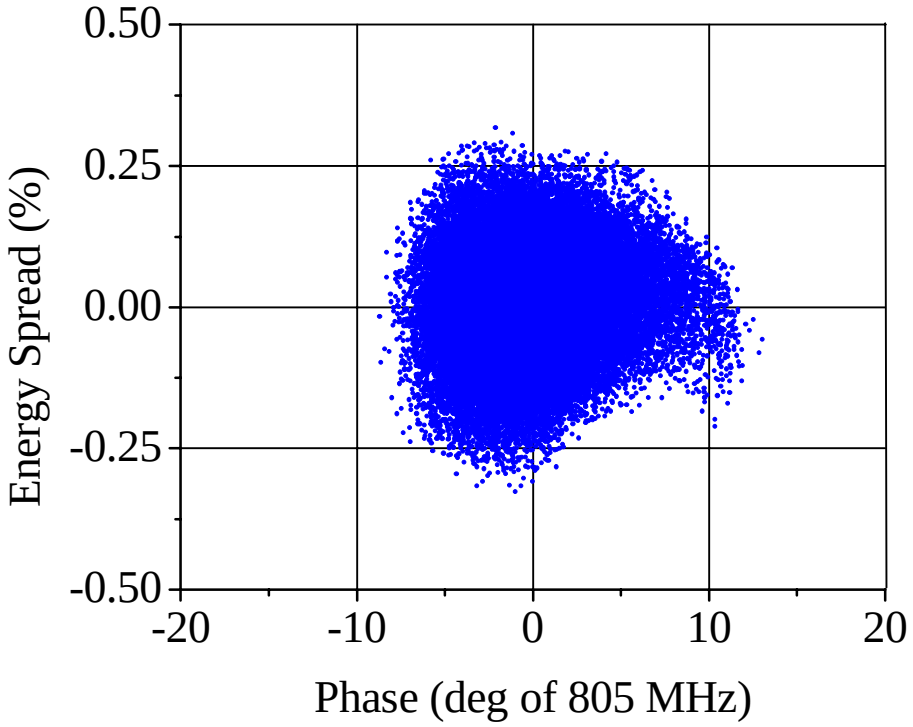

System for selecting multiple q state beams through a 180° bend at 80 MeV/u.

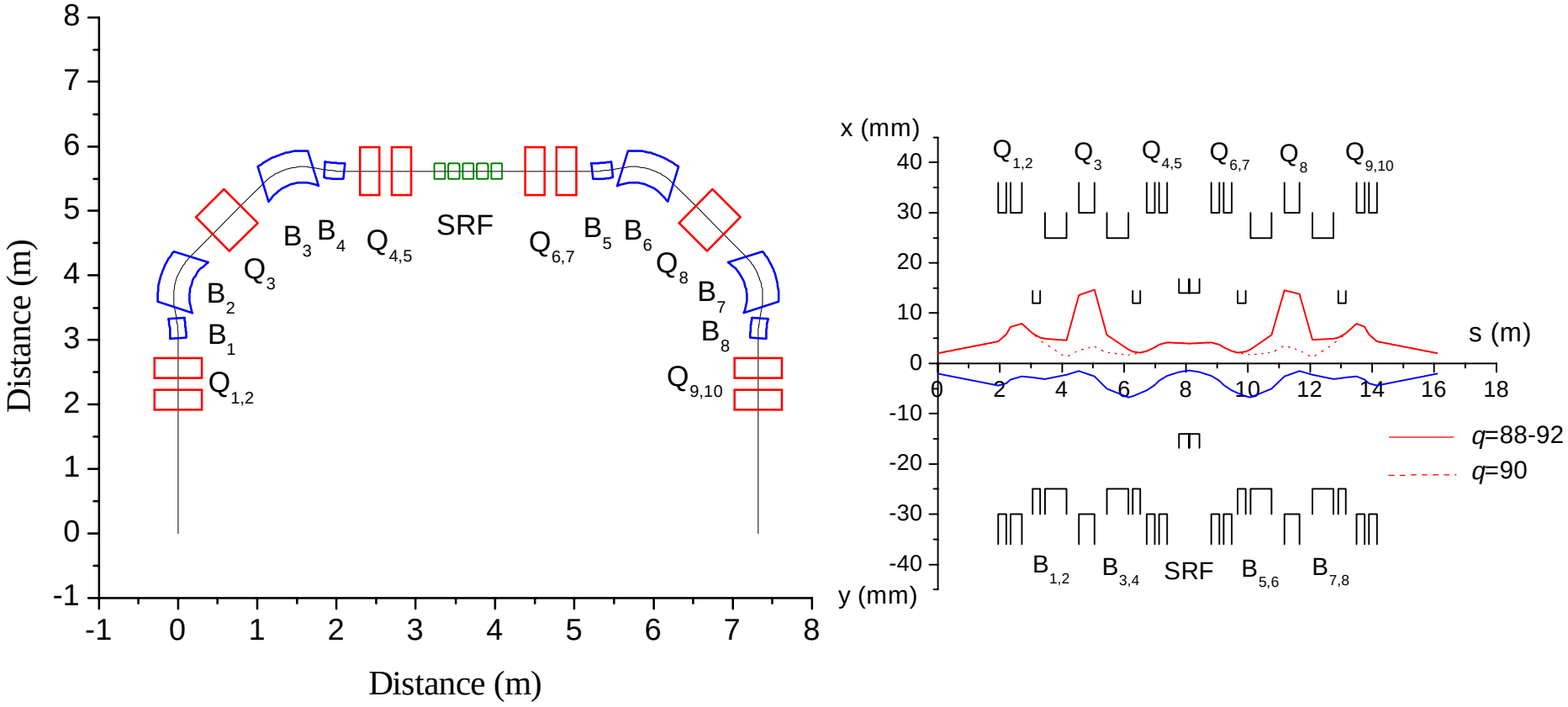

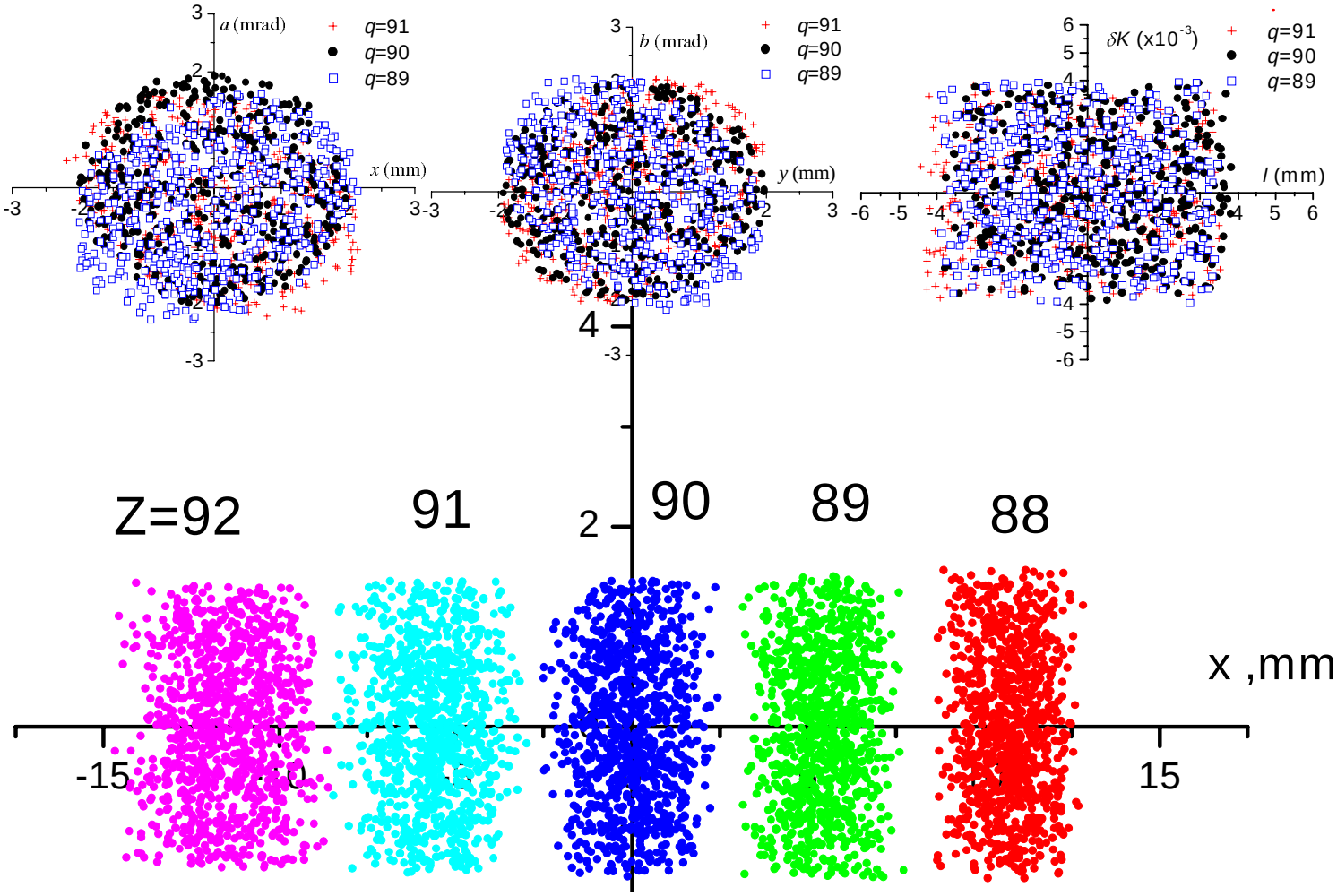
a (mrad)
q=91
q=90
q=89
x (mm)
b (mrad)
y (mm)
δK (x10-3)
l (mm)
Z=92
91
90
89
88
x ,mm
-15
15

Main sources of longitudinal emittance growth:

- Multiplicity of charge state (different synchronous phase, frequency jumps);
- Random errors of rf field;
- Passage through the stripper;
- Coupling of r-z motion in the RFQ.

Main sources of transverse emittance growth:

- Coherent oscillations of multi-q beams due to the misalignment of focusing elements;
- Mismatch of multi-q beam;
- Passage through the stripper;
- Higher-order distortions in the post-stripper transport systems.

RMS emittance growth of multi-q uranium beam in the driver Linac

	Transverse	Longitudinal
Low-β	1.80	1.12
Stripper 1	1.06	1.1
Medium-β	1.95	5.24
Stripper 2	1.12	1.04
High-β	1.05	1.83
TOTAL	4.4	12.3

Triple Spoke vs Elliptical

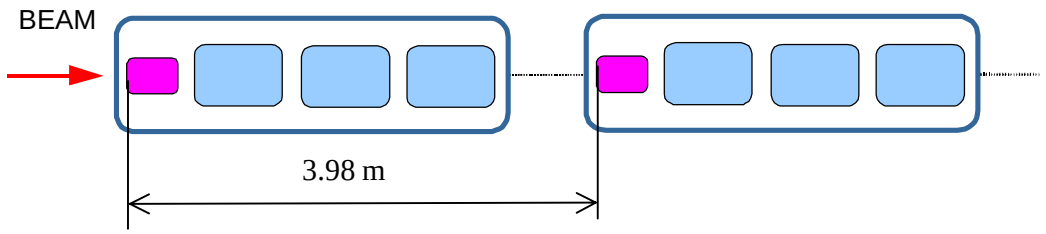

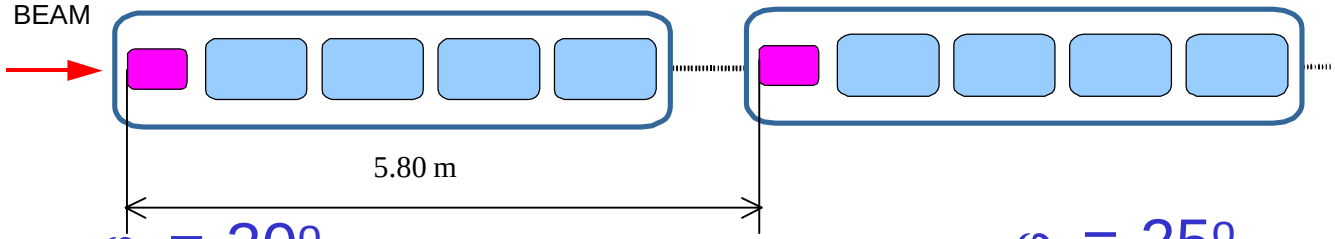

φ_S=-30º

φ_S=-25º

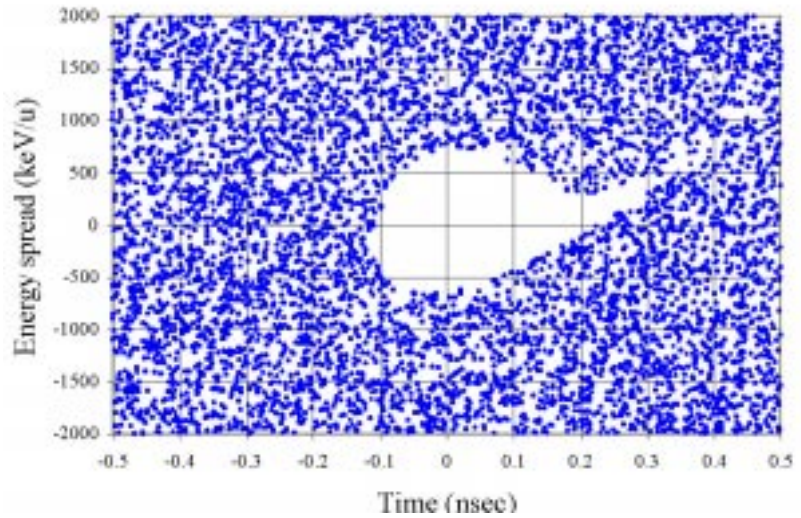

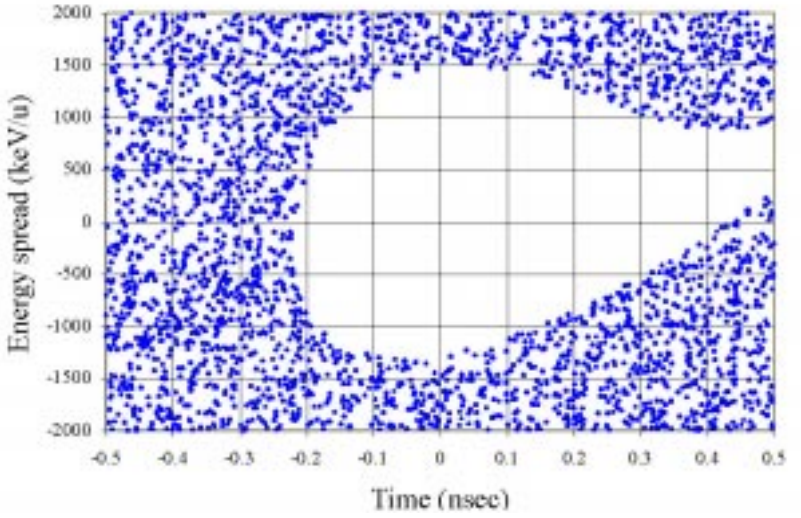

Triple Spoke vs Elliptical

	ECL	TSCL
Number of cavity types	3	2
Peak surface field (MV/m)	27.5	28.
Frequency (MHz)	805	345
Total number of cavities	188	140
Number of cryostats (focusing periods)	47	38
Length in the tunnel (m)	260	200
Operating temperature (°K)	2.1	4.5
Synchronous phase (deg)	-30	-25
Longitudinal acceptance (keV/u-nsec)	60	280
Aperture diameter (mm)	80	40
Transverse normalized acceptance (π mm-mrad)	70	35

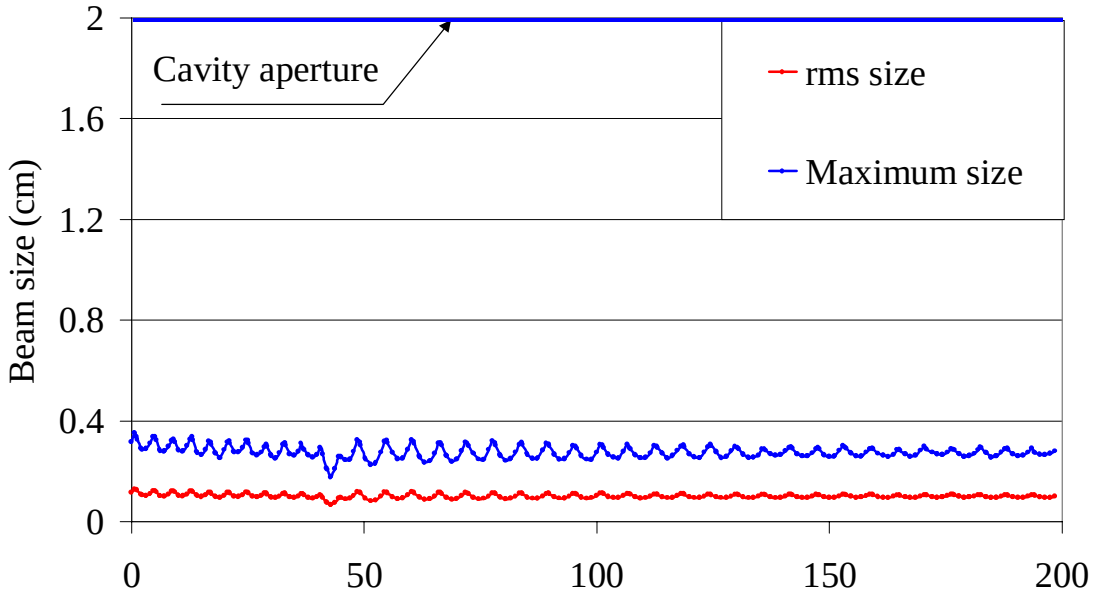
Cavity aperture
rms size
Maximum size
Beam size (cm)
2
1.6
1.2
0.8
0.4
0
0
50
100
150
200
Distance (m)

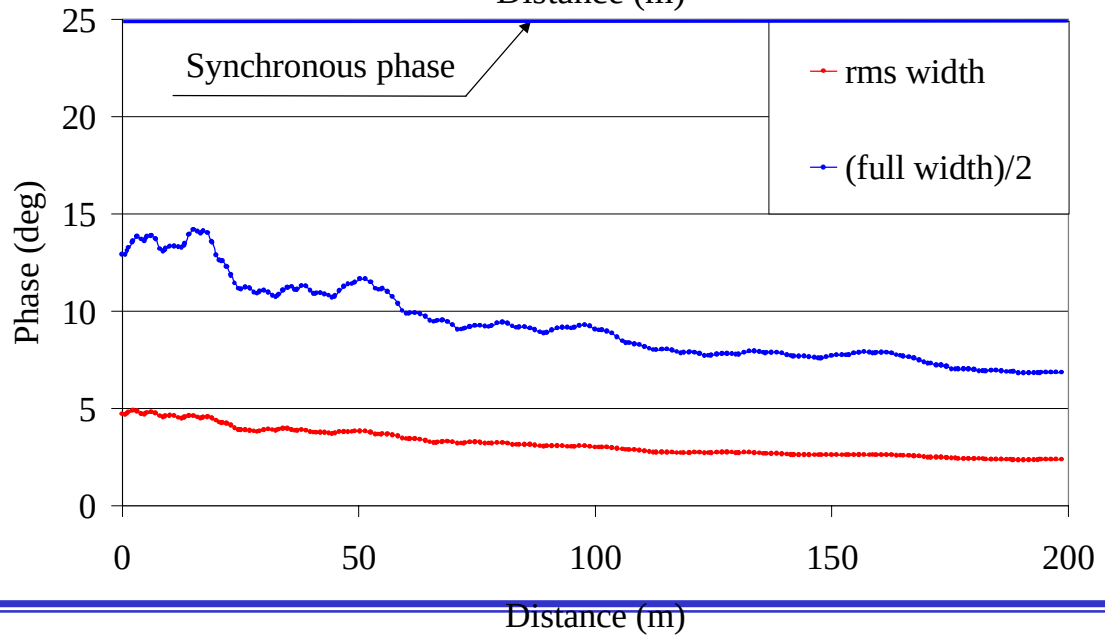
Synchronous phase
rms width
(full width)/2
Phase (deg)
25
20
15
10
5
0
0
50
100
150
200
Distance (m)

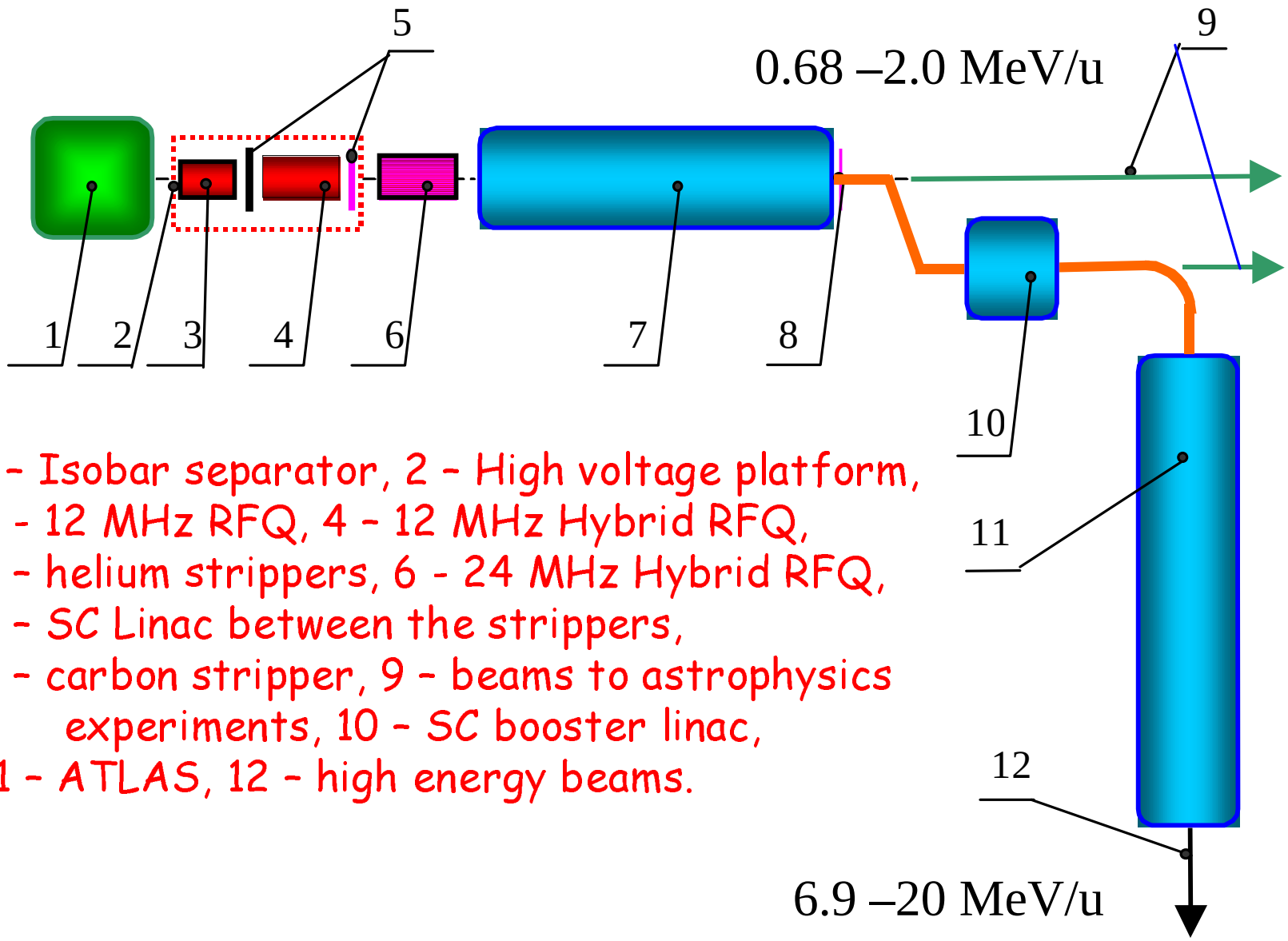

1 – Isobar separator, 2 – High voltage platform,
3 - 12 MHz RFQ, 4 – 12 MHz Hybrid RFQ,
5 – helium strippers, 6 - 24 MHz Hybrid RFQ,
7 – SC Linac between the strippers,
8 – carbon stripper, 9 – beams to astrophysics experiments, 10 – SC booster linac,
11 – ATLAS, 12 – high energy beams.

Accelerating structure for the Hybrid-RFQ, f=12.125 MHz

$^{240}U^{+1}$

V=100 kV

$P_{calculated}$=11 kW

L=3.5 m

W_{inj}= 7 keV/u

W_{exit}=22 keV/u

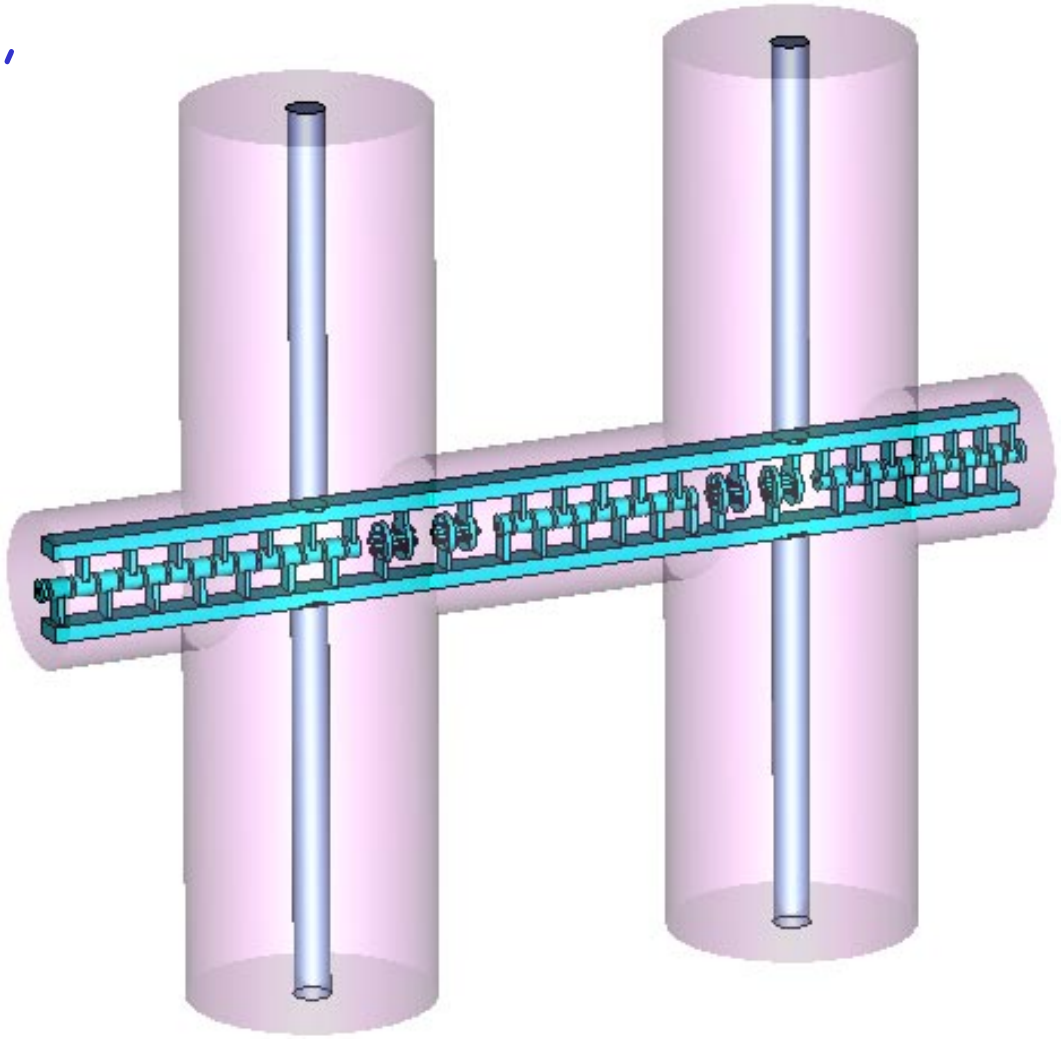

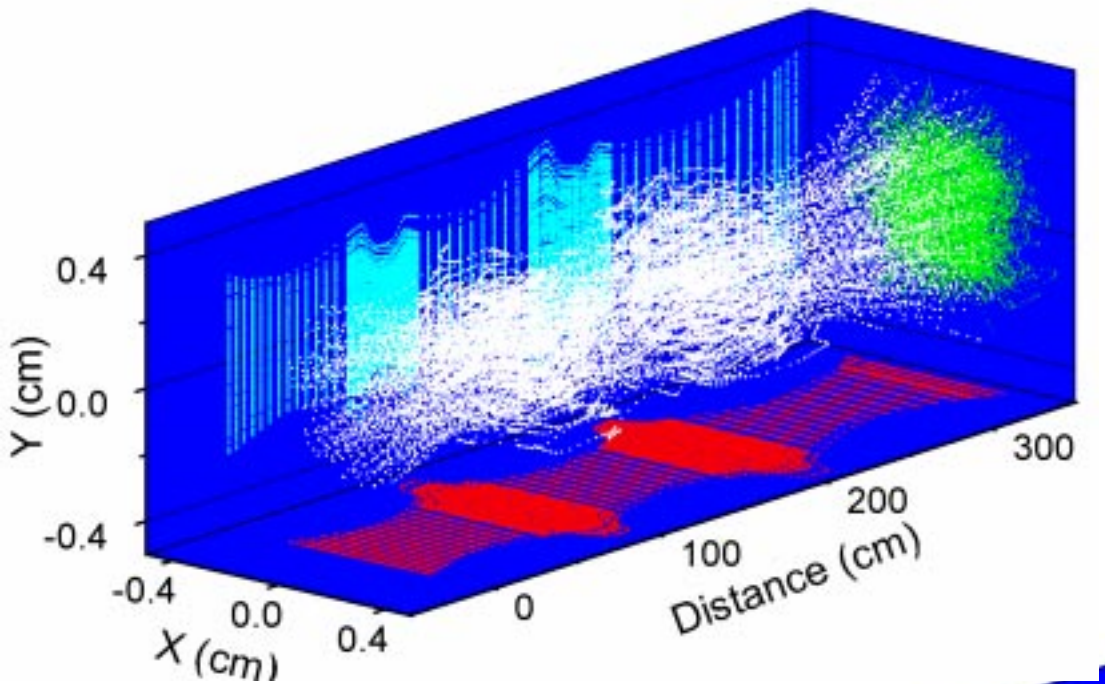

Particle trajectories in the Hybrid RFQ

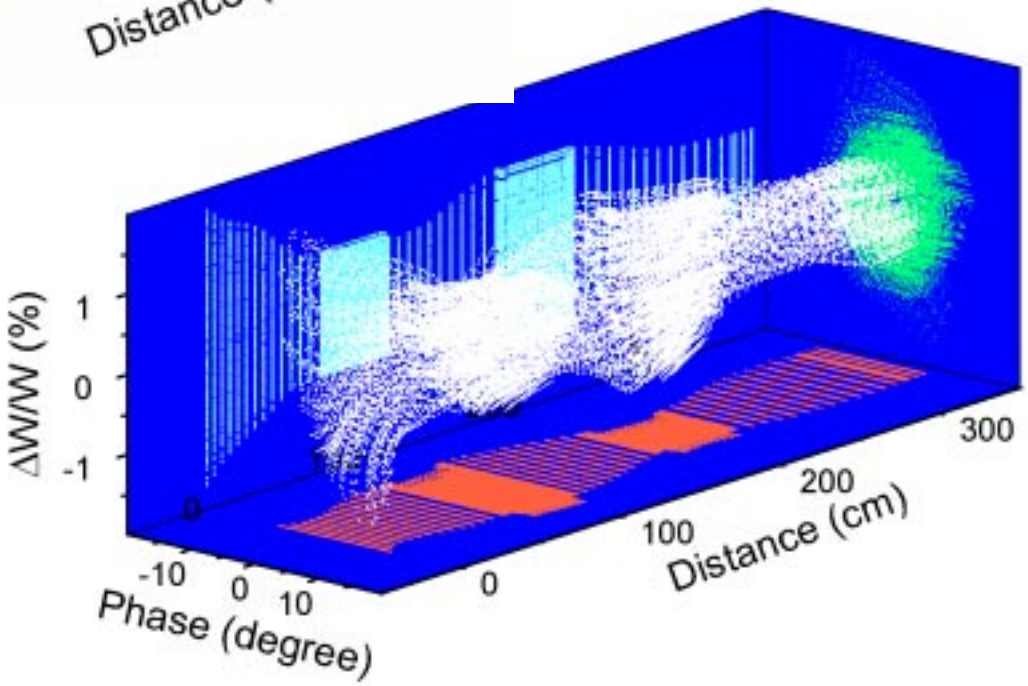

Summary

- The technique of multi-q beam acceleration and transport is understood well;
- A detailed design has been developed for the focusing-accelerating lattice of the RIA accelerators;
- Substantial progress has been made in beam dynamics studies in the SRF DTL;
- Detailed BD studies in the driver linac taking into account errors and misalignments have been carried out;
- Several design concepts related to the driver linac have been successfully tested on the existing SC linac ATLAS.